Molecular Recognition and Self-Assembly by Non-amidic Hydrogen Bonding. An Exceptional "Assembler" of Neutral and Charged Supramolecular Structures†

Stephen Hanessian,* Michel Simard, and Stefano Roelens*,‡

Contribution from the Department of Chemistry, Université de Montréal, P.O. Box 6128, Succursale Centre-ville, Montréal, Québec, Canada H3C 3J7

Received January 26, 1995®

Abstract: The two enantiomers of *trans*-1,2-diaminocylohexane form well-defined supramolecular structures with appropriately paired C_2 symmetrical 1,2-diols that are assembled by H-bonding. Depending on the structure and chirality of the diol, it is possible to form left- or right-handed trihelicate structures consisting of polar cores and hydrophobic outer residues. These structures can be sublimed without change, and they slowly adsorb carbon dioxide to eventually give polymeric amorphous fibers. Heating these materials regenerates the original 1:1 adducts as supramolecular entities. The parent diamines can be converted into crystalline carbamate salts which exist as layered trihelicate structures. Other charged supramolecular structures are formed from the (*R,R*)-diamine and the enantiomeric tartaric acids. The diamine molecule appears to be a superb assembler of neutral and charged supramolecular structures by accommodating preferred diol and acid partners in its crystal lattice. Molecular recognition and self-assembly are based on non-amidic H-bonding between amine and alcohol functions in the neutral molecules, leading to supramolecular structures whose helicity mode depends on the sense of chirality of the diamine used. All the reported structures were characterized by single-crystal X-ray analysis.

Introduction

The design and preparation of stable, higher-order solid-state structures capable of discrete existence solely based on noncovalent interactions is one of the fundamental tenets of supramolecular chemistry.[1] The construction of a variety of organized molecular frameworks, often with potentially useful physical and chemical properties, has in fact, become a most challenging research endeavor.[2] Indeed, the engineering of solid-state superstructures[3] can be considered as a form of chemical artwork, masterfully conceived by the human mind, and often supervened by the subtle yet overwhelming physical forces that ultimately decide the architecture and aesthetic quality of the resulting product. It is in fact widely accepted that predictions of crystal structures from a knowledge of chemical composition of component molecules are far from being realized by intuition, by design, or by other physical principles.[4] The situation is even more complicated in the case of spontaneous organization leading to three-dimensional arrays.

Hydrogen bonding has been a singularly important principle in the design of a variety of supramolecular assemblies.[2,3,5] In addition to being one of the strongest intermolecular forces, H-bonds are directional, a feature that can be modulated with the choice of donor-acceptor species. Nature, in fact, offers the most ingenious examples of utilizing these properties.[5b] It is not surprising therefore that H-bonding involving neutral amidic-type NH and carbonyl-type O atoms has played a prominent role in the design of unique self-assembling supramolecular structures.[6,7] Weak as they are compared to covalent bonds, such intermolecular forces utilizing H-bonding can result in the formation of stable, highly organized single supramolecular entities.[6] Because spontaneous organization and coherence are invariably involved, such intermolecular forces must dominate kinetic energy. The congruence of steric compatibility with favorable geometry during self-assembly is responsible for the generation of order on a macromolecular scale.

Although the interaction between simple amines and alcohols has been demonstrated spectroscopically,[8] and analytically,[9] the possibility of generating self-assembled supramolecular struc-

† Dedicated to Professor Albert Eschenmoser on the occasion of his 70th birthday, wishing him the best in chemistry and in life.

‡ Permanent address: CNR, Centro di Studio sulla Chimica e la Struttura dei Composti Eterociclici e loro Applicazioni, Dipartimento di Chimica Organica, Università di Firenze, I-50121 Firenze, Italy.

® Abstract published in *Advance ACS Abstracts*, June 15, 1995.

(1) Lehn, J.-M.; *Angew. Chem., Int. Ed. Engl.* **1990**, *29*, 1304; **1988**, *27*; 89. Vögtle, F. *Supramolecular Chemistry*; John Wiley & Sons Ltd.: Chichester, U.K., 1991.

(2) Mascal, M. *Contemp. Org. Synth.* **1994**, *1*, 31.

(3) (a) Desiraju, G. R. *Crystal Engineering: The Design of Organic Solids*; Elsevier: New York, 1989. (b) Di Salvo, F. J. *Science* **1990**, *247*, 649. (c) Aakeröy, C. B.; Seddon, K. R. *Chem. Soc. Rev.* **1993**, *22*, 397.

(4) For pertinent references on predictions of crystal structures, see: (a) Reference 3a, Chapters 1 and 5. (b) Perlstein, J. *J. Am. Chem. Soc.* **1994**, *116*, 455; **1992**, *114*, 1955. (c) Gavezzotti, A. *J. Am. Chem. Soc.* **1991**, *113*, 4622; *Acc. Chem. Res.* **1994**, *27*, 309. (d) Etter, M. C. *Acc. Chem. Res.* **1990**, *23*, 120. (e) Maddox, J. *Nature* **1988**, *335*, 201. (f) Leiserowitz, L.; Hagler, A. T. *Proc. R. Soc. London, A* **1983**, *388*, 133. (g) Curtin, D. Y.; Paul, I. C. *Chem. Rev.* **1981**, *81*, 525.

(5) For authoritative references, see: (a) Reference 3a, Chapter 5. (b) Jeffrey, G. A.; Saenger, W. *Hydrogen Bonding in Biological Structures;* Springer-Verlag: Berlin, 1991. (c) Pauling, L. *The Nature of the Chemical Bond*, 3rd ed.; Cornell University Press: Ithaca, NY. 1960.

(6) For selected recent references, see: (a) Khazanovich, N.; Granja, J. R.; McRee, D. E.; Milligan, R. A.; Ghadiri, M. R. *J. Am. Chem. Soc.* **1994**, *116*, 6011. (b) Mathias, J. P.; Simanek, E. E.; Whitesides, G. M. *J. Am. Chem. Soc.* **1994**, *116*, 4326. (c) Mathias, J. P.; Simanek, E. E.; Zerkowski, J. A.; Seto, C. T.; Whitesides, G. M. *J. Am. Chem. Soc.* **1994**, *116*, 4316. (d) Yang, J.; Marendaz, J.-L.; Geib, S. J.; Hamilton, A. D. *Tetrahedron Lett.* **1994**, *35*, 3665. (e) Chang, Y.; West, M.; Fowler, F. W.; Lauher, J. W. *J. Am. Chem. Soc.* **1993**, *115*, 5991. (f) Lehn, J.-M.; Mascal, M.; DeCian, A.; Fisher, J. *J. Chem. Soc., Perkin Trans. 2* **1992**, 461. Simard, M.; Su, D.; Wuest, J. D. *J. Am. Chem. Soc.* **1991**, *113*, 4696 and references cited therein.

(7) For crystallographic studies, see: Taylor, R.; Kennard, O. *Acc. Chem. Res.* **1984**, *17*, 320. See also ref 3a, Chapter 5.

(8) See for example: (a) Tubergen, M. J.; Kuczkowski, R. L. *J. Am. Chem. Soc.* **1993**, *115*, 9263. (b) Edlund, U.; Holloway, C.; Levy, G. C. *J. Am. Chem. Soc.* **1976**, *98*, 5069. (c) Joesten, M. D.; Schaad, L. J. *Hydrogen Bonding*; M. Dekker, Inc.: New York, 1974.

0002-7863/95/1517-7630$09.00/0

tures based on intermolecular H-bonding between mutually compatible partners had not been demonstrated until very recently.[10]

Thus, provided that stable entities can be produced, the interaction between a chiral amine and a chiral alcohol could vastly expand the realm of possibilities for designing functionally and topologically novel if not unique supramolecular motifs. The solution to this provocative hypothesis might lie in the judicious choice of chiral amine and alcohol partners in which the individually encoded stereochemical information (*recognition*) can work in concert with the functional and steric complementarity (*organization*) to provide the necessary driving force for self-assembly. Although far from being predictable, a natural consequence of the above-mentioned issues could be the formation of discrete, metal-free three-dimensional higher-order structural motifs with peculiar tertiary structures.[11]

To experimentally explore the validity of these hypotheses, it was imperative that we select amines and alcohols with elements of symmetry that would be conducive to the formation of ordered networks, hopefully in crystalline form. Our long-standing interest in the synthesis and utilization of C_2 symmetrical vicinal *trans*-1,2-diamines[12] and -1,2-diols,[13] in asymmetric reactions, coupled with a series of serendipitous laboratory observations, and a recent report by Kawashima, Hirata, and Hirayama,[14] instigated a systematic study of the problem.

We report in this paper details of our recently communicated results[10] on the nature of supramolecular motifs formed between (*R,R*)- and (*S,S*)-1,2-diamino cyclohexanes and (*S,S*)-1,2-cyclohexanediol. Furthermore, we extend this study to include other diols as well as charged species, all of which form self-organized and highly ordered assemblages that are admirably suited for X-ray crystallographic analysis. Although X-ray crystallography was imperative in determining the three-dimensional structures of the motifs described in this paper, *discussion will be focused mainly on the nature of the motifs, on some unusual physicochemical properties, and on the prospects of understanding the factors that govern the type and shape of H-bonded arrays.*[15]

Results

Neutral Networks. When a suspension containing equimolar amounts of enantiomerically pure (1*S*,2*S*)-1,2-diaminocyclohexane, **1**, and (1*S*,2*S*)-1,2-cyclohexanediol, **2**, in benzene was brought to the reflux temperature of the solvent, and the clear solution allowed to cool, a crystalline product was formed quantitatively (Scheme 1). Spectroscopic analysis revealed the formation of a 1:1 adduct, **3**, mp 78−79 °C, which was soluble in halogenated hydrocarbons and in toluene, but rapidly dissociated to its components in protic solvents. The same behavior was exhibited by the enantiomeric diamine **4**, which gave a crystalline adduct, **5**, mp 63−65 °C. X-ray structure analysis of adducts **3** and **5** unambiguously showed the formation of a 1:1 complex consisting of one molecule each of diamine and diol in each case, and linked by a pair of interactions well within the distance of a definite H-bond. When a sample of **1** was heated in benzene with an equimolar amount of racemic *trans*-1,2-cyclohexanediol, a solid containing the diol **2** with an enantiomeric enrichment of about 67% crystallized out of solution.[14] Further recrystallization allowed an enrichment to ca. 80% ee. Slight differences in H-bonding distances and angles[15] account for the different melting points and solubilities in benzene, hence the enantiomeric enrichment reported by Kawashima and co-workers.[14]

Scheme 1

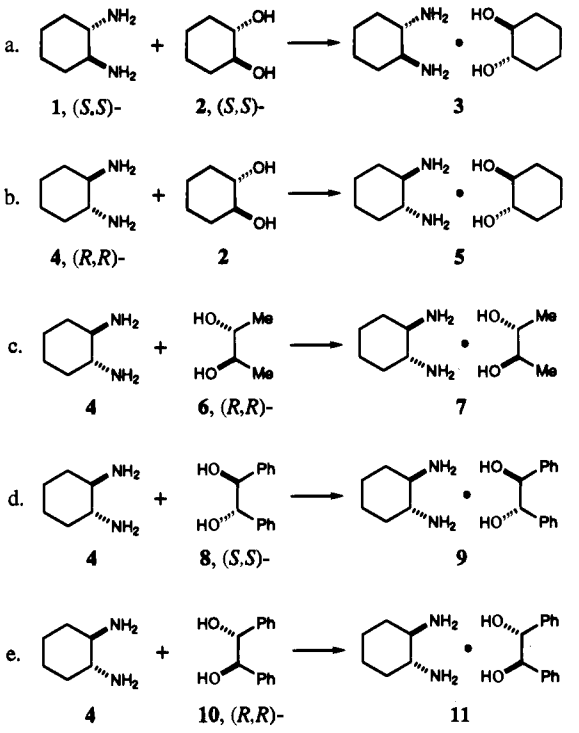

Adducts **3** and **5** form unprecedented, well-defined, and extremely ordered supramolecular structures that appear to spontaneously self-assemble through a unique network of H-bonds. A peculiar feature of such assemblies is the alignment of the cyclohexane rings of both reagents into four vertical columns with the polar groups facing inward. The result is a central core with a pleated sheet-like array, much like a staircase, and consisting of eight-membered, square planar, H-bonded units. These involve two fully tetracoordinated amino groups and two fully tetracoordinated hydroxy groups from two pairs of diamine and diol molecules (Figure 1B,E). The remaining functional groups are engaged in two symmetrical side rows of H-bonds which flank opposing sides of the central staircase core and join amine and alcohol groups in a zigzag pattern (Figure 1C,F). Unlike the central core, the side-row H-bonding occurs through tricoordinated oxygen on alternating diol units. The nitrogen atom of the intervening diamine unit is tricoordinated because of the inaccessibility of a second hydrogen atom for coordination. Except for this amino group, all other hydrogens

(9) Pirkle, W. H.; Pochapsky, T.-C. *Chem. Rev.* **1989**, *89*, 347. Weisman, G. R. In *Asymmetric Synthesis*; Morrison, J. D., Ed.; Academic Press: New York, 1983; Vol. 1, p 153.

(10) (a) Hanessian, S.; Gomtsyan, A.; Simard, M.; Roelens, S. *J. Am. Chem. Soc.* **1994**, *116*, 4495. (b) For an intersting perspective, see: Ermer, O.; Eling, A. *J. Chem. Soc., Perkin Trans. 2* **1994**, 925.

(11) For selected examples of metal-containing helical assemblies, see: Bell, T.W.; Jousselin, H. *Nature* **1994**, 367, 441. Carina, R. F.; Bernardinelli, G.; Williams, A. F. *Angew. Chem., Ind. Ed. Engl.* **1993**, *32*, 1463. Constable, E. C.; Edwards, A. J.; Raithby, P. R.; Walker, J. V. *Angew. Chem., Int. Ed. Engl.* **1993**, *32*, 1465. Potts, K. T.; Horwitz, C. P.; Fessak, A.; Keshavarz, K. M.; Nash, K. E.; Toscano, P. J. *J. Am. Chem. Soc.* **1993**, *115*, 10444. Ghadiri, M. R.; Soares, C.; Choi, C. *J. Am. Chem. Soc.* **1992**, *114*, 825. Bernardinelli, G.; Piguet, C.; Williams, A. F. *Angew. Chem., Int. Ed. Engl.* **1992**, *31*, 1622. Garrett, T. M.; Koert, U.; Lehn, J.-M.; Rigault, A.; Meyer, D.; Fischer, J. *J. Chem. Soc., Chem. Commun.* **1990**, 557. Koert, U.; Harding, M. M.; Lehn, J.-M. *Nature* **1990**, *346*, 339.

(12) Hanessian, S.; Gomtsyan, A. *Tetrahedron Lett.* **1994**, *35*, 7509. Hanessian, S.; Gomtsyan, A.; Payne, A.; Hervé, Y.; Beaudoin, S. *J. Org. Chem.* **1993**, *58*, 5032. Hanessian, S.; Bennani, Y.; Hervé, Y. *Synlett* **1993**, 35. Hanessian, S.; Beaudoin, S. *Tetrahedron Lett.* **1992**, *33*, 7655, 7659. Hanessian, S.; Bennani, Y. *Tetrahedron Lett.* **1990**, *31*, 6465 and previous references.

(13) Hanessian, S.; Meffre, P.; Girard, M.; Beaudoin, S.; Sancéau, J.-Y.; Bennani, Y. *J. Org. Chem.* **1993**, *58*, 1991.

(14) Kawashima, M.; Hirayama, A. *Chem. Lett.* **1991**, 763; **1990**, 2279. Kawashima, M.; Hirata, R. *Bull. Chem. Soc., Jpn.* **1993**, *66*, 2002.

(15) Complete X-ray crystallographic and spectroscopic data are provided in the supporting information.

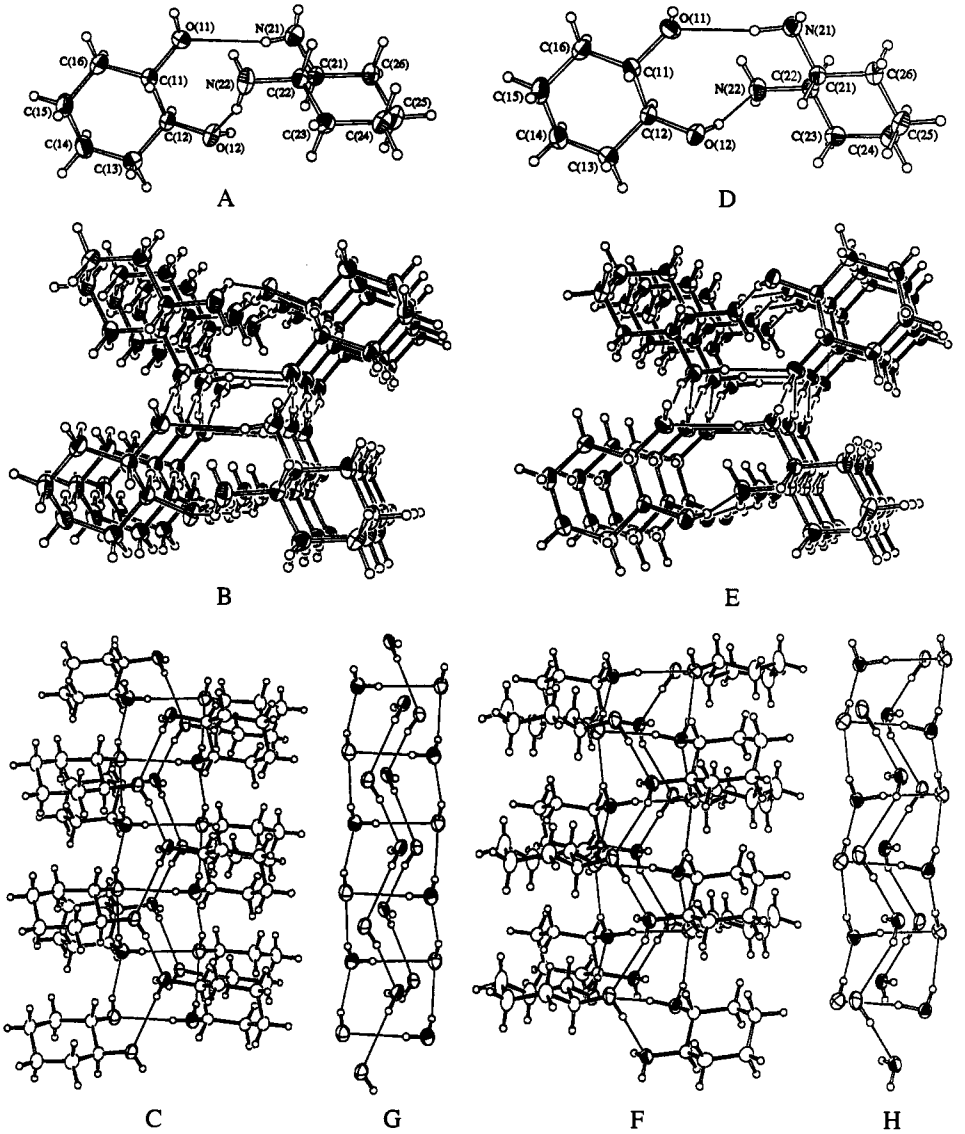

Figure 1. (A, D) ORTEP views of the molecular structure of adducts **3** and **5**, respectively (H-bonds are represented by thin lines). (B, E) H-bonding network for **3** and **5** (top view down the *a* axis). (C, F) Side view of the H-bonding network of **3** and **5**. (G, H) Simplified depiction of the views in (C) and (F) showing the pleated sheet motif of the core and the side rows of H-bonds. It is apparent that the superstructures of **3** and **5** are closely related.

on the hetero atoms are engaged in a *fully hydrogen-bonded supramolecular structure*. Infrared spectra of **3** and **5** in KBr exhibit extensive H-bonding compared to the diamine or diol progenitors alone.[16] The entire set of hydrogen bond distances ranges from 1.87 to 2.37 Å for **3** and from 1.88 to 2.42 Å for **5**. The homochiral and heterochiral complexes appear to be comparable crystallographically. However, closer scrutiny reveals several interesting features associated with the H-bonded array. Thus, **3** and **5** have virtually identical staircase-like cores and side rows with alternating H-donation between oxygen and nitrogen. However, the relative sense of donation in the core is *opposite* to that in the side rows in **3** and in **5**. This intriguing feature can be visualized by examining the partial structures of G and H in Figure 1.

A remarkable consequence of H-bonding in these three-dimensional assemblies is the emergence of a tertiary structure in which the diamine−diol components wrap around the central core in a triple-stranded helicate (Figure 2, top left and right). These superstructures constitute unique examples of metal-free helicates that are *self-assembled by simple H-bonding between amine and alcohol groups*. It is equally remarkable that the sense of chirality for both homochiral and heterochiral adducts is determined by the chirality of the diamine. Thus, whereas the (*S,S*)-enantiomer **1** gives a left-handed helicate, **3**, with the (*S,S*)-diol, the (*R,R*)-enantiomer **4** gives a right-handed helicate, **5**, with the same diol. In each case, a full turn comprises four units, involving a pair each of alternating diamines and diols.

Three strands run parallel in the helicate at a fixed distance so that the groove of the helix is one-third of the pitch (Figures 2 and 3). The strands are held together by alternate H-bonds of the staircase and the side rows along the network axis. The remaining alternate H-bonds of the core and of the side rows interlink single molecules in each strand. The perpendicular H-bonds of the staircase fix the gauge of the helix, thus rendering the helicate completely rigid. The pitch of the helix spanning two starter units at the beginning and end of a full turn (e.g., diols A_1, A_2, A_3, etc.) is 15.724 Å in **3** and 15.048 Å in **5** (Figure 3). The distances (grooves) between each unit and its immediate "lower" or "higher" like neighbor are 5.241 and

(16) For studies with vicinal diols, see: Huang, C.; Cabell, L. A.; Anslyn, E. V. *J. Am. Chem. Soc.* **1994**, *116*, 2778. For FTIR studies on hydrogen bonding in amides, see: Dado, G. P.; Gellman, S. H. *J. Am. Chem. Soc.* **1993**, *115*, 4228. For reviews of the use of IR spectra in connection with H-bonding, see: Symons, M. C. R. *Chem. Soc. Rev.* **1983**, *12*, 1. Aaron, H. S. *Top. Stereochem.* **1979**, *11*, 1. See also ref 8c.

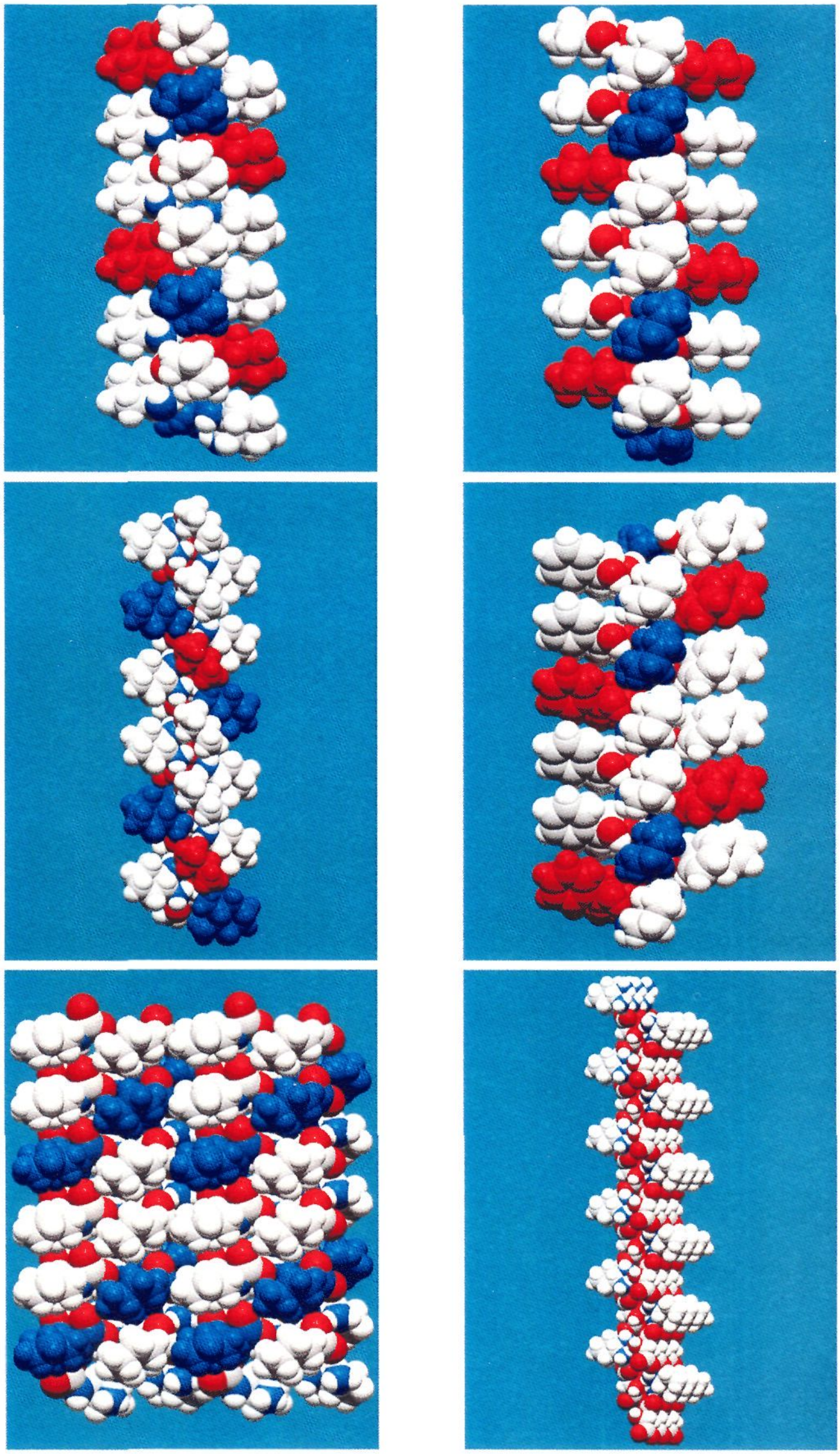

Figure 2. CPK representation of the triple-stranded helical tertiary structures of **3** (top left), **5** (top right), and **7** (middle left) and corresponding right-handed pseudotrihelicate structure of **9** (middle right). Diamine residues are shown in blue and diols in red within one strand of the trihelicates in **3**, **5**, **7**, and **9**. For **12** (bottom left), a segment showing two contiguous elements of the layered structure is depicted, with diamines in blue and carboxylate oxygen atoms in red. The CPK representation of the layered structure of **13** (bottom right) shows the "shelf-like" motifs of the diamine molecules on layers of tartrate molecules, with oxygen in red and nitrogen in blue.

5.016 Å, respectively. The outer gauge between diamine residues is 13.22 Å in **3** and 13.25 Å in **5**, while the distances between diol units in **3** and **5** are 13.74 and 14.29 Å, respectively. The left-handed helix of the homochiral complex

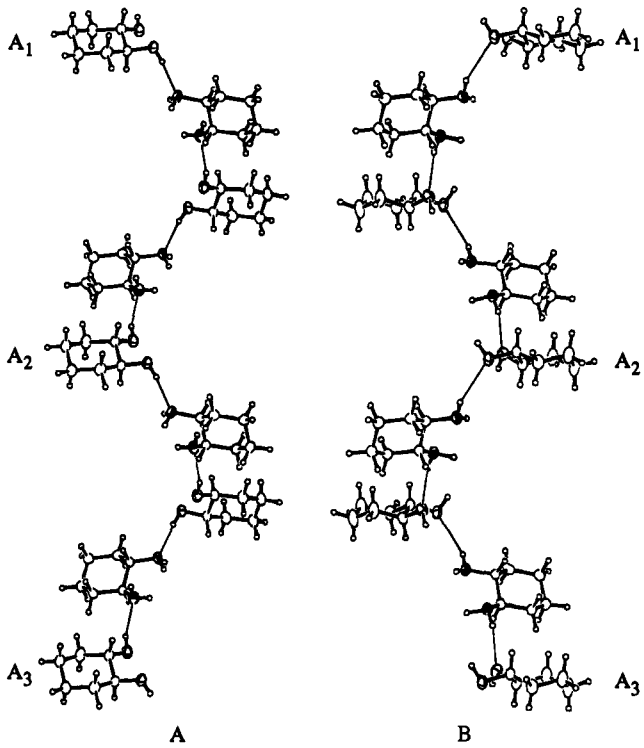

Figure 3. (A) Single strand of H-bonded diamine and diol units extracted from the triple-stranded helicate structure of the adduct **3**. H-bonds are homogeneously formed between OH donors and NH_2 acceptors. A1, A2, and A3 indicate repeating diol units after a full turn and denote the pitch of the helix. (B) Same view as (A) of the adduct **5**. In this case, H-bonds are homogeneously formed between OH acceptors and NH_2 donors. A1, A2, and A3 represent repeating diol units.

3 is therefore longer and narrower than the right-handed helix of the heterochiral counterpart **5** as can be appreciated from the CPK representations in Figure 2.

The donor−acceptor roles of hydroxy and amino groups in these structures present some fascinating features of mutual complementarity. In general, H-bonding is shared equally between nitrogen and oxygen in **3** and **5**, each behaving as donors and acceptors with full tetracoordination in the staircase-like core. Tricoordinated nitrogen and oxygen atoms are also linked by equally shared H-bonds in the side rows, except for one unshared NH group pointing inward (Figure 1B,E). Within the edges of the core and the side rows, H-bonds are *homodromic*, running in the same direction but with opposite senses relative to each other (Figure 1G,H). H-bonds constituting the strands in **3** are formed between *oxygen donors and nitrogen acceptors only*, providing a left-handed helical periphery that joins the amine and diol units (Figure 3A). In **5**, however, the right-handed helical peripheral motif consists of H-bonds in which *nitrogen is the donor and oxygen is the acceptor* (Figure 3B). The direction of H-bonding in the strands of **3** and **5** is *antidromic*, running in an opposite sense from donors to acceptors. Hydrogen bonds of the strands are characterized by N···O distances of 2.787 and 2.985 Å for **3** and 3.203 and 3.280 Å for **5**, which lie in the range of typical H-bonding distances. H-bonds from O donor to N acceptor are shorter in **3** (2.13 and 1.93 Å) compared to those seen in **5** from N donor to O acceptor (2.43 and 2.42 Å) (Figure 3). Crystallographic data pertaining to data collection and structure refinement are listed in Table 1.[15]

The interchangeable donor−acceptor interactions observed in the solid state for **3** and **5** were also confirmed by ^1H NMR spectroscopy in benzene or toluene solution,[15] with the observation of downfield shifts for both *CH*OH and *CH*NH_2 signals.

It is noteworthy to mention that the full tetracoordination of both nitrogen and oxygen atoms in the core portion of **3** and **5** (Figure 1C,F) is not found in the X-ray crystal structures of the diamine **1** or the diol **2**. These individually consist of a zigzag "planar" network held together by H-bonds between the amino groups and hydroxy groups within each series.

The relative stability of the three-dimensional structure in **3** was most surprising in view of the fact that the solid material or a melted sample could be cleanly sublimed at 45−50 °C and 1.5 Torr, giving a crystalline sublimate identical to **3** quantitatively. This demonstrates the great propensity for self-assembly during the short-path sublimation process. At this point, it cannot be ascertained if the superstructure dissociates into smaller sublimable units, or if individual amine and diol components are produced initially, and recombined to reconstitute the original assembly. In either case, the process leads to the same ordered structure as evidenced by an X-ray analysis of the sublimate.

In an attempt to extend the scope of such phenomena involving H-bonding interactions, we examined the interactions between other pairs of C_2 symmetrical, enantiomerically pure diamines and diols. Initial results utilizing (1*R*,2*R*)-1,2-diphenylethylenediamine, and (2*R*,2′*R*)-2,2′-diaminobinaphthyl as diamine components with a number of diols failed to afford solid adducts suitable for X-ray studies. We then returned to **1** and **4** as the diamines of choice, and we studied their adducts with a number of readily available C_2 symmetrical diols.[14]

Equimolar amounts of **4** and (2*R*,3*R*)-2,3-butanediol, **6**, afforded a crystalline adduct, **4**, from benzene (Scheme 1). In contrast to all other adducts examined, the melting point of this complex, 65−67 °C, was higher than that of both its progenitors (diamine mp 41−43 °C; diol, liquid), which was suggestive of stronger H-bonding compared to the individual reagents. Indeed, the X-ray crystal structure exhibits a vast H-bonding network, through which a three-dimensional structure self-assembles along the *a* crystallographic axis (Figure 4A). Cyclohexane and methyl residues are stacked in four columns as was found for **3** and **5**, although the structure is markedly more tilted (Figure 4B). The hydrogen-bonding motif of the core is not a pleated sheet as previously observed for **3** and **5**, but rather a right-handed helical ribbon, consisting of eight-membered square planar hydrogen bonded units, and wrapped around the axis of the assembly (Figure 4C). The most remarkable feature of the adduct **7** is that the folding of the above ribbon into the observed helical motif allows for an *unprecedented full coordination of all the heteroatoms in the structure*, which is most likely the driving force of the folding process. Furthermore, the double-stranded helical pattern of the hydrogen bonds constituting the edges of the ribbon represents, to the best of our knowledge, *the first example of a self-assembled hydrogen-bonded coil* involving amino and hydroxyl groups exclusively. The network defines a rigid, roughly cylindrical channel of 4.2−4.4 Å diameter along the *a* axis (Figure 4A) where the distances between all the opposite nitrogen (4.814 Å) and oxygen (5.066 Å) atoms are quite similar. In contrast, the pleated sheet-like core of **3** and **5** exhibited a somewhat rectangular section, with distances between opposite oxygen (4.601 Å in **3** and 4.776 Å in **5**) and nitrogen atoms (**3**, 4.217 Å; **5**, 3.992 Å) comparable to those in **7**. The remaining opposite pairs of oxygen and nitrogen atoms belonging to the side rows exhibit markedly longer distances because of the

Table 1. Crystallographic Data Collection and Structure Refinement Information[a]

	3	**5**	**7**	**9**	**11**	**12**	**13**	**14**
space group	$P2_12_12_1$	$P2_12_12_1$	$I2_12_12_1$	$P2_1$	$P2_1$	$P2_1$	$P2_1$	$P2_1$
Z	4	4	4	2	2	4	2	2
cell constants								
a, Å	5.2412(10)	5.016(2)	6.7643(16)	11.986(4)	11.7443(14)	12.252(3)	5.5427(13)	8.3022(6)
b, Å	11.9046(10)	11.898(2)	6.7643(16)	5.9230(17)	5.3002(12)	5.086(3)	10.196(2)	7.1761(8)
c, Å	21.4921(22)	22.675(7)	16.533(4)	12.748(4)	14.7768(12)	13.047(3)	10.920(2)	12.3089(10)
β, deg	90.00	90.00	90.00	93.70(2)	93.360(8)	91.876(18)	95.694(17)	102.079(6)
V, Å^3	1341.0(3)	1353.3(7)	1309.1(6)	903.1(5)	918.2(3)	812.6(6)	614.1(2)	717.10(11)
μ, mm^{-1}	0.58	0.57	0.54	0.58	0.57	0.75	0.96	0.99
D_{calcd}, g/cm^3	1.141	1.131	1.037	1.208	1.188	1.293	1.429	1.391
$F(000)$	512	512	456	356	356	344	284	324
radiation	Cu Kα_1	Cu Kα_1	Cu Kα_1	Cu Kα_1	Cu Kα_1	Cu Kα_1	Cu Kα_1	Cu Kα_1
θ_{max}, deg	70.0	70.0	70.0	70.0	70.0	70.0	70.0	70.0
scan mode	$\omega-2\theta$	$\omega-2\theta$	$\omega-2\theta$	$\omega-2\theta$	$\omega-2\theta$	$\omega-2\theta$	$\omega-2\theta$	$\omega-2\theta$
h,k,l ranges	+6,+14,+26	+6,+14,+27	+8,+14,+20	±14,+7,+15	±14,+6,+18	±14,+6,+15	±6,+12,+13	±10,+8,+14
no. of reflns measd	9846	10065	4787	6727	6858	5728	4556	5342
no. of unique reflns	1515	1527	729	1890	1947	1721	1235	1476
R_{merge}	0.027	0.015	0.031	0.018	0.053	0.042	0.075	0.021
no. with $I > 1.96\sigma(I)$	1424	1278	665	1816	1909	1615	1188	1441
no. of params	251	249	114	330	330	310	243	278
R_f	0.035	0.033	0.032	0.032	0.028	0.034	0.043	0.029
R_w	0.039	0.036	0.035	0.040	0.036	0.041	0.052	0.035
GoF	2.22	1.45	1.77	2.57	2.61	1.89	3.01	2.28

[a] $R_f = \Sigma(||F_o| - |F_c||)/\Sigma(|F_o|)$. $R_w = [\Sigma w(|F_o| - |F_c|)^2/\Sigma(w|F_o|)^2)]^{1/2}$. GoF $= [\Sigma w(|F_o| - |F_c|)^2/(\text{no. of reflns} - \text{no. of params})]^{1/2}$.

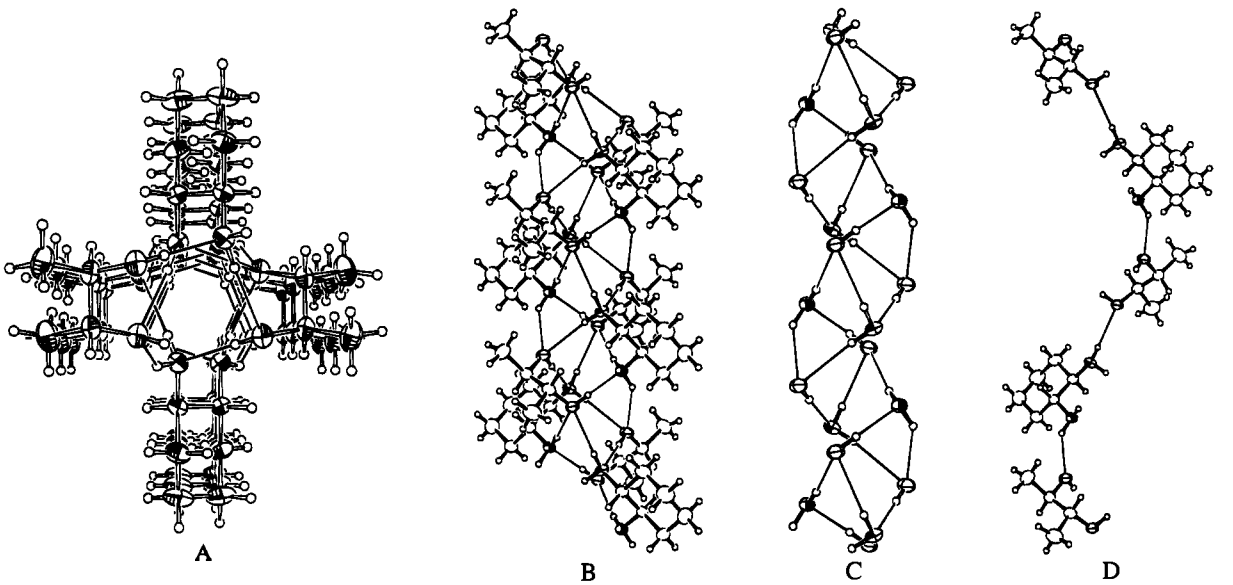

Figure 4. (A) H-bonding network of the adduct **7** (top view down the *a* axis). (B) Side view of the H-bonding network (H-bonds represented by thin lines) showing the full coordination of all heteroatoms. (C) Simplified representation of the view in (B) showing the right-handed helical motif of the pleated sheet ribbon constituting the H-bonded core of the assembly. (D) Single strand of H-bonded units extracted from the triple-stranded helicate structure in **7** showing left-handed helicity. H-bonds are uniformly established between NH_2 donors and OH acceptors of alternate diamine and diol molecules.

instability of the core to fold helically about the axis (oxygen atoms 7.358 Å in **3** and 7.998 Å in **5**; nitrogen atoms, 6.104 Å in **3** and 6.138 Å in **5**).

The three-dimensional H-bonding array present in **7** revealed some fascinating symmetry features. Thus, the H-bonds constituting the edges of the ribbon run in donating directions opposite to each other (antidromic), as do face-to-face perpendicular H-bonds in the ribbon. The result is an alternate rotational and mirror symmetry of hydrogen-bonding directions of contiguous square units. Interestingly, the diamine and diol residues also wrap around the core in a helical fashion, similar to **3** and **5**, but with a much steeper slope. Three antidromic hydrogen-bonded strands run parallel at a distance of 6.764 Å, generating a helicate of 20.293 Å pitch, considerably longer than those of **3** and **5** (15.724 and 15.048 Å, respectively) (Figure 4D).

As mentioned above, fully coordinated nitrogen and oxygen atoms share equivalent and interchangeable donor–acceptor capabilities throughout the H-bonded network in **7**. A remarkable consequence is the emergence of unusual topographical features in the superstructure. Thus, while the peripheral residues consisting of diamine and diol motifs adopt a left-handed helix, the ribbon-like motif within the core has an opposite helicity (Figure 4C,D). The beautiful triple-helicate structure of **7** can be appreciated in the CPK reproduction of the X-ray structure (Figure 2, middle left). Crystals of the adduct **7** could be cleanly sublimed as in the case of **3** and **5**, giving a sublimate that was crystallographically identical to the initial adduct.

Both enantiomers of hydrobenzoin afforded crystalline complexes **9** and **11** with **4**. Unlike **5**, the adduct **9** between the (*R,R*)-diamine **4** and the (*S,S*)-diol **8** showed a higher melting

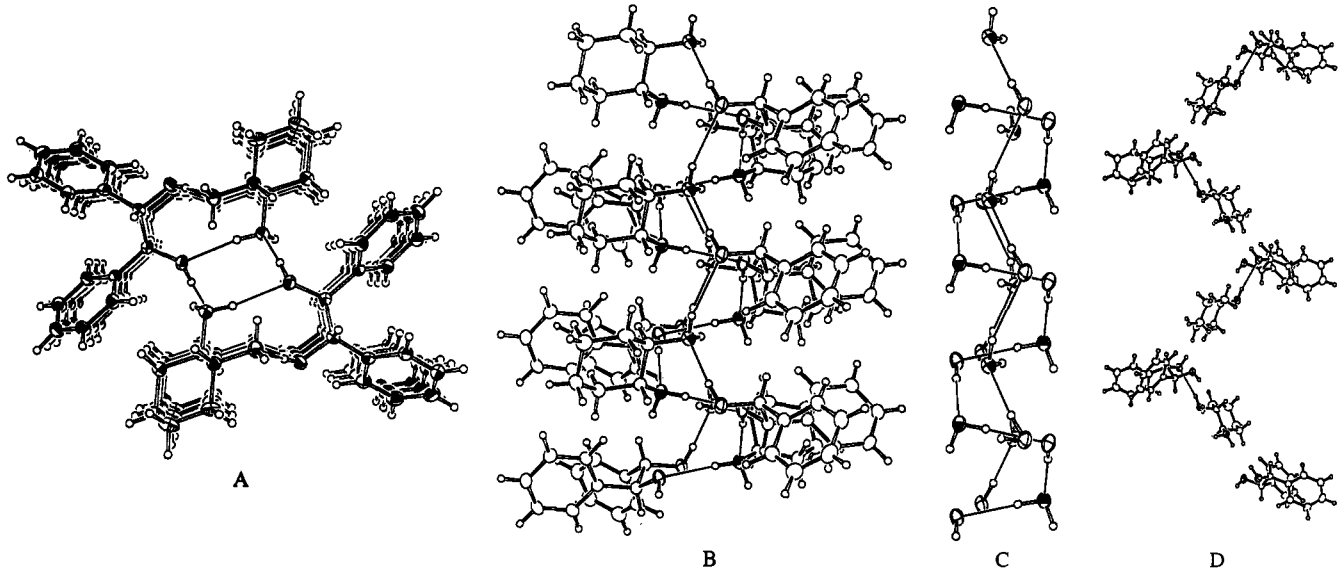

Figure 5. (A) H-bonded assembly of the adduct **9** (top view down the *b* axis). (B) Side view of the assembly (H-bonds represented by thin lines). (C) Simplified representation of the view in (B) showing the "S"-shaped motif of the H-bonded core due to incompletely formed H-bonds of a pleated sheet. (D) Single strand of partially H-bonded diamine and diol units extracted from the structure of adduct **9**. The arrangement of the units in combination with the direction of the H-bonds (thin lines) imparts the right-handed helical shape of the strand, producing a pseudotrihelicate structure.

point (99−100 °C) and lower solubility than its diastereomeric counterpart **11** (mp 75−76°C). This suggested a better matching of partners and stronger H-bonding in the former than in the latter. Such anticipation was confirmed by X-ray crystal structure analysis, which revealed two differently hydrogen-bonded assemblies for the two compounds. The crystal structure of **9** shows the typical staircase-like motif of the H-bonded core previously observed in **3** and **5** (Figure 5A,B). The section across the staircase is similar but slightly larger than those of **3** and **5** with distances of 4.223 and 4.983 Å between opposite pairs of nitrogen and oxygen atoms, respectively. Moreover, some hydrogen bonds are looser with respect to the above-described networks, resulting in a *partially formed staircase* (Figure 5C). In particular, NH···O hydrogen bonds are longer (2.48 Å), affecting the core to a greater extent than the side rows, so that not all NH_2 groups of the core are fully H-bonded to oxygen. The staircase turns into an S-shaped pattern of bonds with skipped NH···O bonds. Longer H-bonds of NH donors had already been noted in the strands of **3** and **5** although the origin could not be ascertained. It now appears that increasing steric congestion in the structure affects nitrogen as a donor more markedly than oxygen. While the overlaying of cyclohexane rings is evident, the phenyl rings line up strongly tilted in four vertical columns, so that π-stacking does not seem to be involved (Figure 5B). The arrangement of diamine and diol residues in **9** can be envisaged as a tertiary structure consisting of a right-handed trihelicate (Figure 5D). Three parallel strands of diamine−diol sequences can be envisaged with their residues coiling around the core at a distance of 5.3 Å from each other. The pitch of the resulting helicate is 15.9 Å, a value notably similar to those characterizing the helices of the other assemblies, **3** and **5**, with staircase-like cores. However, in contrast to **3** and **5** whose trihelicate structures consist of continuously H-bonded residues within the single strands (Figure 3A,B), the heteroatoms in the strands of **9** are not fully linked due to a longer distance between donor nitrogen and acceptor oxygen along the edge of the core. Thus, in the case of **9**, the external residues forming the strands can be construed as assuming the "shape" of a triple-stranded helix (Figure 1D), aided in part by the right-handed direction of the nitrogen to oxygen H-bond linking each neighboring partner in the assembly. In other words, the superstructure **9** is a pseudotrihe-

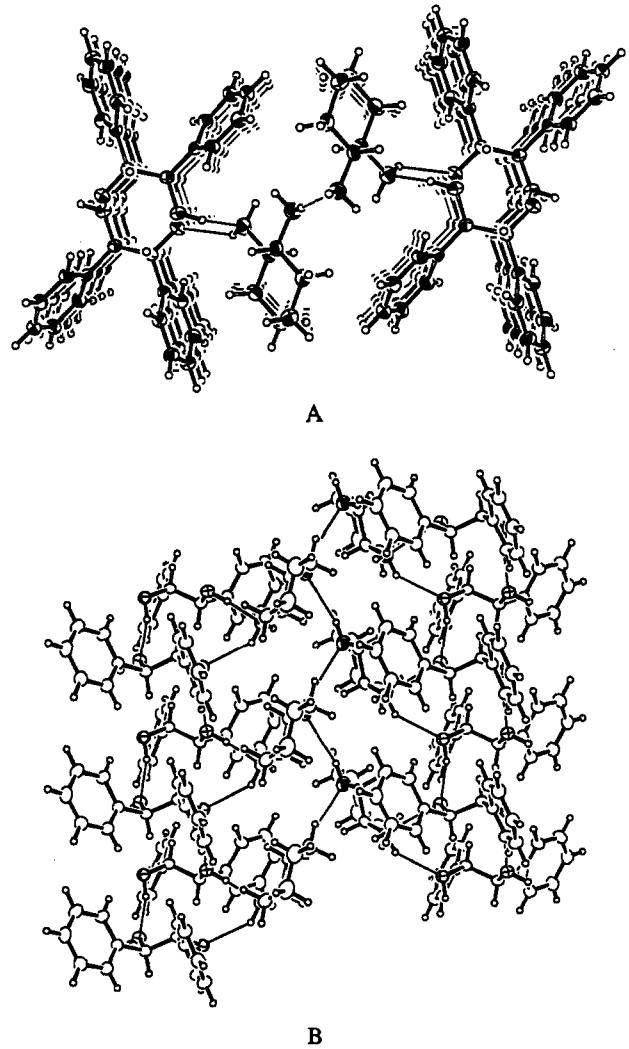

Figure 6. (A) Top view of the assembly of **11** down the *b* axis (the first dimension of the layered structure), showing a segment of the layer taken from the *c* axis (the second dimension). The structure is discrete along the *a* axis. (B) Side view of the assembly down the *a* axis. A section of the layer is shown with H-bonds in thin lines.

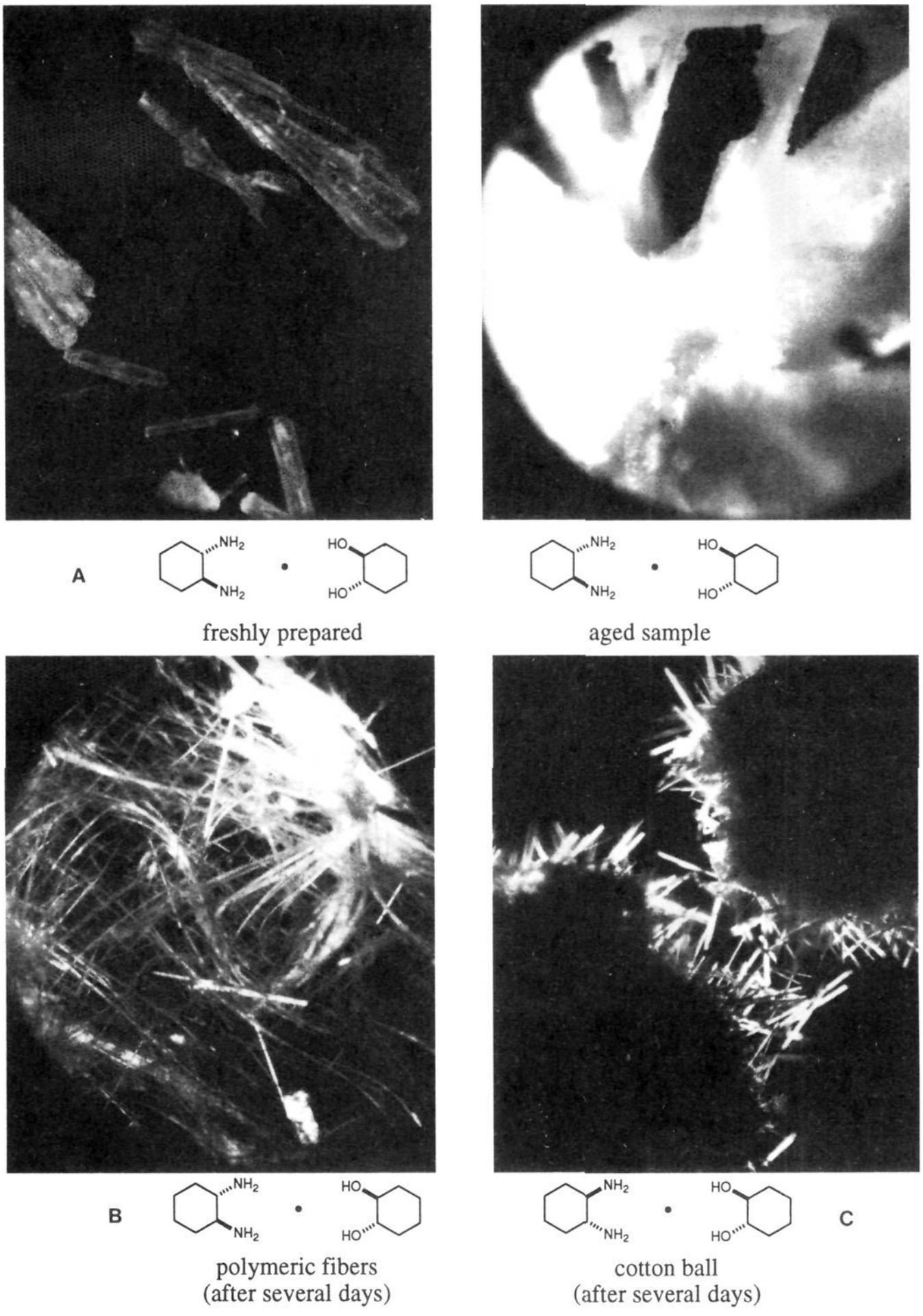

Figure 7. (A) Crystals of freshly prepared adduct **3**. (B, C) Crystals of **3** and **5**, respectively, after several days of exposure to air. (D) Crystals of **3** after prolonged exposure to air.

licate, having the shape but not the H-bonded connectivity of the other trihelicates. A CPK representation of the right-handed pseudotrihelical structure of **9** is shown in Figure 2 (middle right).

A different architecture is exhibited by the crystal structure of **11** (Figure 6) where H-bonding develops along two directions, generating a layered structure. The diamine−diol adduct is held together by only one hydrogen bond, involving one oxygen donor and one nitrogen acceptor. The top view of the network (Figure 6A) shows a new motif consisting of alternating pairs of diamines and diols, which belong to contiguous adducts, interlinked face to face by H-bonds between the remaining hydroxy and amino groups of the partners. Such a sequence gives origin to one dimension of the layer along the *c* axis while the second grows perpendicularly, parallel to the piles of cyclohexane and phenyl rings along the *b* axis. Along this direction, the assembly is threaded by NH···N hydrogen bonds joining diamine molecules, and by alternate O−H−O and O−H−N hydrogen bonds interlinking diamines and diols. This pattern is perceived from the side view of the network, which is the actual plane of the layer (Figure 6B). Hydrogen bonding is undoubtedly the driving force responsible for self-assembly, since all the piled hydrocarbon residues are strongly tilted and stacking interactions likely play a minor role in the process. It is worth noting that **11** is the first assembly of the diamine−diol series studied thus far that consists of a H-bonded network involving *tri*coordinated heteroatoms exclusively.

Charged Networks. An unusual observation during our

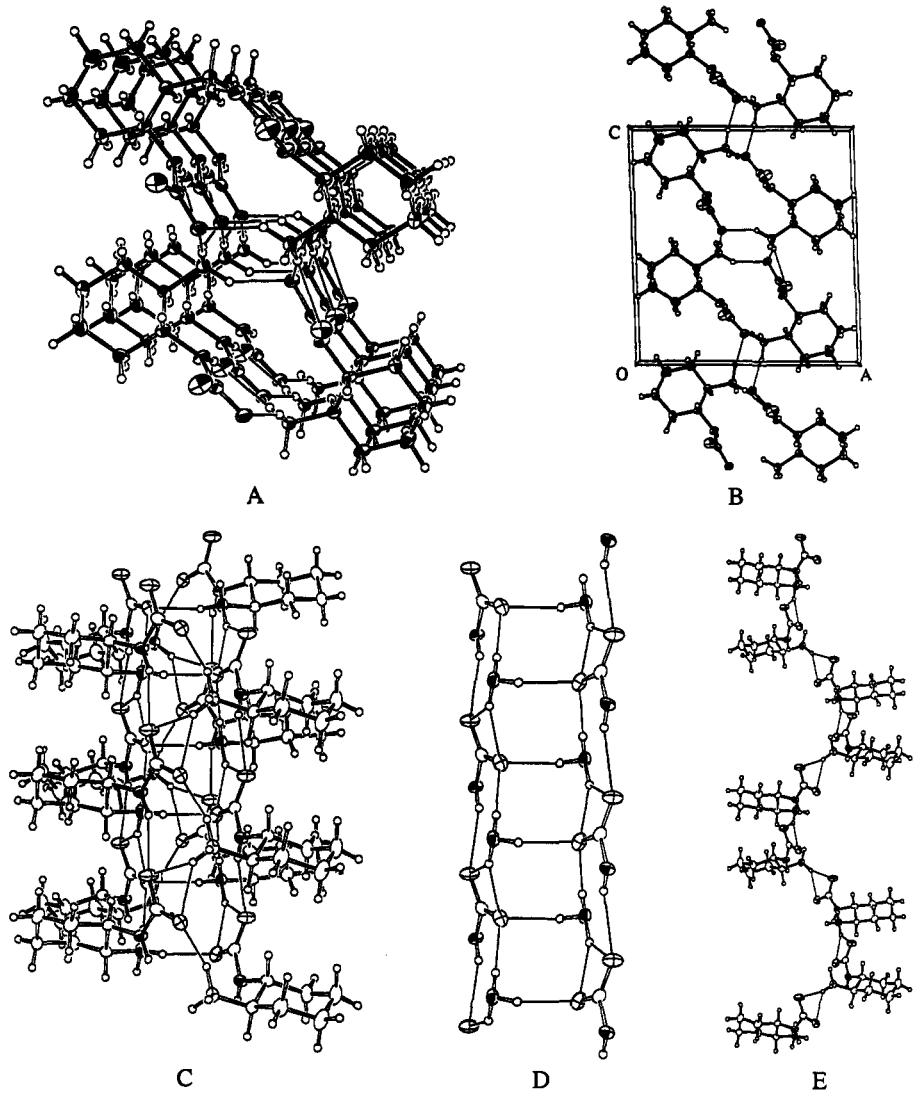

Figure 8. (A) H-bonded assembly (H-bonds represented by thin lines) of the carbamate **12** (top view down the *b* axis). (B) Top view of the cell (down the *b* axis) showing interlinking by H-bonds with contiguous cells along the *c* axis (second dimension of a layered structure). (C) Side view of the assembly down the *c* axis. (D) Simplified representation of the view in (C) showing bifurcated H-bonds and the pleated sheet motif of the fully coordinated H-bonded core. (E) Single strand of diamine and CO_2 units extracted from the triple-stranded helicate structure of a single element of the layered assembly in **12** showing right-handed helicity of the cyclohexane residues.

study of the diamine–diol adducts led to the discovery of novel three-dimensional networks formed between the diamine **1** or **4** and carboxylic acids. Thus, upon exposure to air, X-ray quality crystals of **3** (Figure 7A) eventually became amorphous and did not diffract X-rays anymore (Figure 7D). Powder or microcrystalline samples changed their shape to fiber-like solids (Figure 7B). These changes could be prevented by keeping the crystals under an argon atmosphere and accelerated in the presence of CO_2. Thus, it was clear that the adduct was being carbonated. Heating the carbonated adduct to fusion caused evolution of CO_2 over a wide range of temperatures, leaving behind, after cooling, a solid whose melting point was identical to that of the freshly prepared complex. Thus, these complexes behave as a reversible solid-state CO_2 sponge, and they can be recovered intact after heating and recrystallization.[17] In order to investigate this phenomenon, samples of **3**, **5**, and diamine **4** were artificially carbonated in parallel experiments. The corresponding ^1H and ^{13}C NMR spectra after treatment with CO_2 showed identical signals for the diamine part for the three compounds, while the signals of the diol part of **3** and **5** were the same as those of the unperturbed starting diol. This demonstrated that the chemical behavior of adducts **3** and **5** toward CO_2 is analogous to that of the diamine itself, suggesting that carbonation of the latter is the process responsible for the observed metamorphosis. However, the physical form of the carbonated adduct is unusual and quite different from that of the carbonated diamine. The latter is a stable powder and does not show the formation of the fluffy polymers observed with **3** and **5**. Moreover, the carbonated adducts seem to be much more sensitive to oxidation, becoming dark within weeks, compared to the carbonated diamine, which is stable for longer periods of time.

Although not affecting reactivity toward CO_2, the presence of the diol in the adducts **3** and **5** affects the physical aspect of the carbonated solid and its stability to oxidation. Experiments on diastereomerically pure complexes showed that **5** is much more prone to carbonation and to oxidation compared to **3**. Indeed the former became readily yellow and fluffy, while the latter appeared to be comparatively more stable. Furthermore, **3** developed long polymeric fibers (Figure 7B), while **5** assumed

(17) For other examples of carbamate salts, see: Von Dreele, R. B.; Bradshaw, R. L.; Burke, W. J. *Acta Crystallogr.* **1983**, *C39*, 253. Adams, J. M.; Small, R. W. H. *Acta Crystallogr.* **1973**, *B29*, 2317. Braibanti, A.; Manotti Lanfredi, A. M.; Pellinghelli, M. A.; Tiripicchio, A. *Acta Crystallogr.* **1971**, *B27*, 2261, 2248.

Scheme 2

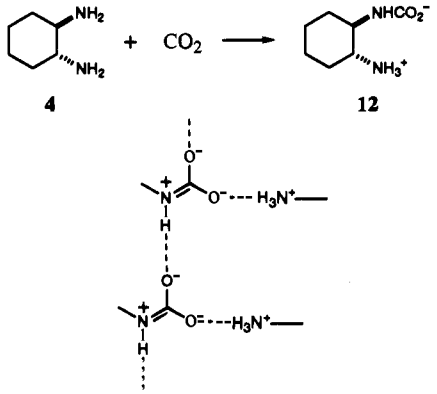

the shape of a cottonball (Figure 7C). Such a difference in shape suggests a different tendency to cross-linking of the two superstructures when reacting with CO_2.

Unfortunately, the products resulting from slow carbonation of the adducts did not provide crystals suitable for X-ray analysis, and their structures could not be assessed. However, the solid obtained by forced carbonation of **3** (mp 132−175 °C, melting with CO_2 evolution) could be crystallized from an ethanol/water mixture to give well-formed crystals. X-ray analysis proved the compound to be the ammonium salt of the carbamic acid generated by the addition of CO_2 to one amino group as in **12** (Scheme 2), the original diol being absent. Indeed, a product of the same structure was independently obtained by carbonation of the diamine **4**. The presence of the diol in the initial carbonated complex may thus be responsible for the formation of fibers (Figure 7B), by means of a three-component H-bonded assembly. Evidently the diol is extruded during crystallization of the carbonated adducts **3** or **5**, and its absence is reflected in the lack of metamorphosis of the new crystals, corresponding to **12**.

The carbamate salt **12** exhibits a new three-dimensional structure that is self-assembled in a two-directional H-bonding network. Although the nature of the hydrogen-bonding interactions involved is markedly different from that of **3**, **5**, and **9**, the top view of the assembly presents a striking similarity to the previously described neutral networks that possess staircase-shaped cores (Figure 8A,B). A pleated sheet-like central core motif, consisting of fused square planar eight-membered hydrogen-bonded units, runs along the vertical *b* axis of the assemblage. Two opposite pairs of ammonium NH and carboxylate oxygen constitute each unit. The third ammonium proton and the second carboxyl oxygen are engaged in a typical bifurcated hydrogen bond that reinforces the core on both sides. The same carboxyl oxygen is also involved in an amidic-type hydrogen bond with the carbamic NH, and gives rise to a pair of parallel, nearly coplanar rows of hydrogen bonds flanking the core. The central pleated sheet and the flanking motifs, alternating four- and eight-membered hydrogen-bonded rings, can be appreciated from the side view of the network (Figure 8C,D). Four piles of carbamate molecules are joined by the core through one of the two functional groups. Cyclohexane rings, perfectly stacked in four columns, encapsulate the polar core in a nonpolar environment. This arrangement describes the constitutive element (Figure 8A) of the layered structure, which develops in the second direction (*c* axis) by H-bonding contiguous elements through the second functional group of each carbamate molecule (Figure 8B). It is noteworthy that such interlinking replicates the basic structural motif of the core, merely rotated by 90° around the vertical *b* axis. Along the second dimension of growth (*c* axis), the network can therefore be described as a double layer of nonpolar residues enclosing a layer of polar cores. *All* the carboxyl oxygen and ammonium nitrogen atoms involved in the hydrogen-bonding motif of the cores are fully tetracoordinated, while those involved in the amidic-type hydrogen bonding in the side rows are tricoordinated, due to the occurrence of bifurcated hydrogen bonds. Such a coordination pattern is analogous to that observed in **3**, **5**, and **9**, although the type of bonds involved is remarkably different.

An impressive feature is the recurrent *helicate arrangement of residues* around the core of each single element of the layer reminiscent of those found in neutral networks. The CPK perspective in Figure 2 (bottom left) shows a side view along the *a* axis of repeating elements, each consisting of triple-stranded helicates with four diamine units per full turn in each single strand. The constitution of each element can also be appreciated in a partial side view along the *c* axis in Figure 8C. The ORTEP representation of a single strand of a single trihelicate with cyclohexane residues wrapped around the central staircase is shown in Figure 8E. It should be noted that the chirality throughout the superstructure is once again governed by the configuration of the parent diamine **1**. Contiguous helicates are hydrogen bonded to each other, producing an assembly that can be viewed as a infinite bundle of triple-stranded helicates fused together in a layered superstructure, much like a stone wall having a symmetrical pattern of inlaid material on both sides.

The intricate three-dimensional structure of **12** can be further appreciated from the perspectives shown in Figure 9. Thus, in Figure 9A we can see a partial structure down the *a* axis that matches the CPK model (Figure 2, bottom left) consisting of diamine units that are joined in a helical manner through carbamic acid bridges. Triple-stranded helical modules are interconnected to each other by a H-bonding pattern showing the familiar staircase motif (Figure 9A,B) identical to the core, but rotated by 90°. Each staircase is the core of a trihelicate joined by "horizontal" $CO_3^-\cdots NH_3^+$ bonds, a pattern which repeats itself along the *c* axis. Figure 9C shows a single strand of each of two contiguous interlinked helicates with typical bifurcated carboxylate bridges.

Tartrate Salts of 4. Both enantiomers of tartaric acid form crystalline salts with **4**, although their physical properties are quite different (Chart 1). The solubility in water of the salt of the natural tartaric acid **13** is markedly lower than that of its diastereomer **14** which allows for a very efficient resolution.[18] The salt formed between **4** and (*R,R*)-tartaric acid, **13**, mp 252−255 °C, exhibits a highly interlinked bidirectional hydrogen-bonding network. The tweezer-shaped motif is the constitutional element of the assemblage (Figure 10A), and it is characterized by H-bonding interactions involving ammonium nitrogen donors and hydroxyl oxygen acceptors. The network develops in a plane perpendicular to the *c* axis of the adduct by hydrogen-bonding carboxylate groups to ammonium ion in one direction and to hydroxyl groups in the other. Canal-like cavities, running inside the core along the *a* axis and delimited by carboxyl, ammonium, and hydroxyl groups, are envisaged from the top view of the assembly (Figure 10A). Their ellipsoidal section has opposite carboxyl O−O, ammonium N−N, and hydroxyl O−O distances of 3.834, 5.351, and 5.042 Å, respectively. The side view of the network along the *b* axis clearly shows a

(18) Hanessian, S.; Delorme, D.; Beaudoin, S.; Leblanc, Y. *J. Am. Chem. Soc.* **1984**, *106*, 5754. Onuma, K.; Ito, T.; Nakamura, A. *Bull. Chem. Soc. Jpn.* **1980**, *53*, 2012. Galsbøl, F.; Steenbøl, P.; Søndergaard, G.; Sørensen, S. B. *Acta Chem. Scand.* **1972**, *26*, 3605. Asperger, R. G.; Liu, C. F. *Inorg. Chem.* **1965**, *4*, 1492. Jaeger, F. M.; Bijkerk L. Z. *Anorg. Allg. Chem.* **1937**, *233*, 97.

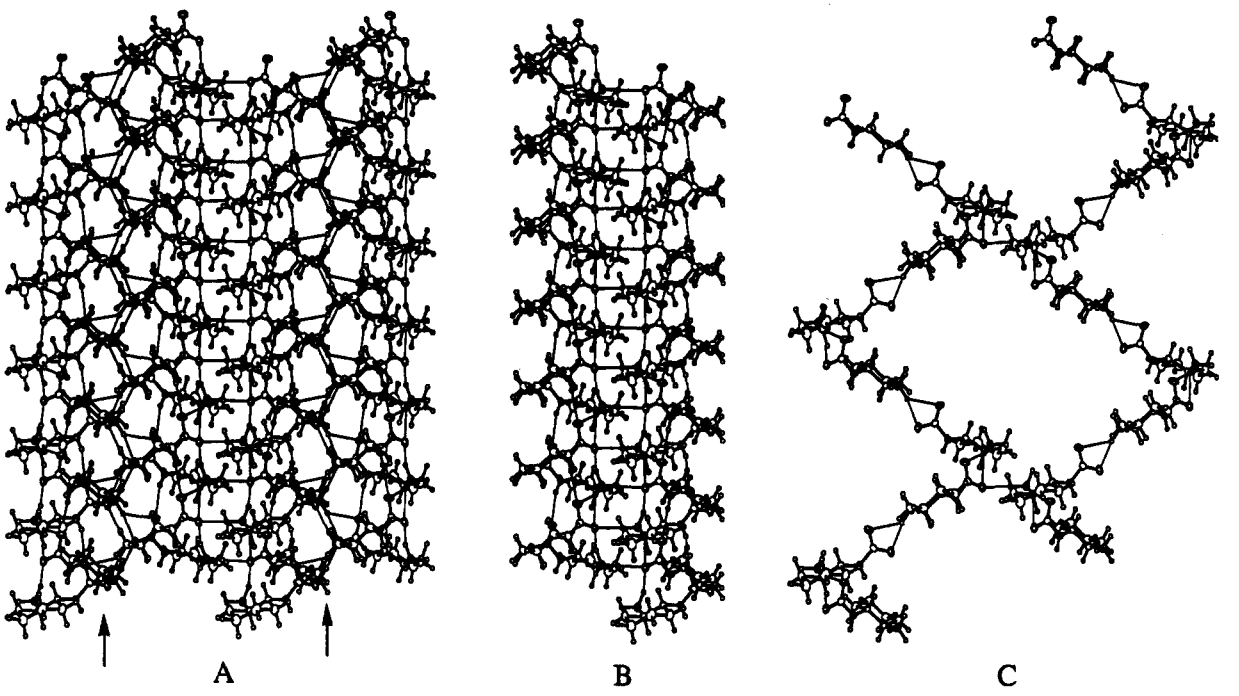

Figure 9. (A) View of **12** down the *a* axis similar to Figure 2D, showing a central staircase that joins elements on either side. Arrows indicate positions of staircase motifs at a 90° angle to the staircase of the central element. (B) Isolated view of the central staircase. (C) Two left-handed helicates joined in the middle by transversal $CO_3^{-}\cdots NH_3^{+}$ bonds that constitute part of the central staircase motif.

Chart 1

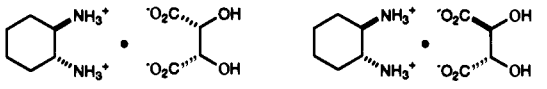

13, (*R,R/R,R*)-

14, (*R,R/S,S*)

"hollow brick" structure of the bilayered core (Figure 10B). The side view along the *c* axis, which is the actual front view of the bilayer, displays the architecture of the hydrogen-bonding network, consisting of 10-membered hydrogen-bonded rings as its constitutional motif (Figure 10C). The net-shaped appearance shows to what extent the term "network" is appropriate to describe this assembly.

As in **12**, the hydrogen-bonding network generates a layered structure in which tartrate units are aligned on a plane, forming a bilayered core. Diamine units are alternately grafted on both sides of the core, with stacks of cyclohexane rings inserted as shelves on a wall. The bilayered core is 3.52 Å thick; the width of the assembly is 11.34 Å, including the cyclohexane residues, and the repeat distance between two "shelves" is 10.20 Å. A CPK representation of such a motif is shown in Figure 2 (bottom right).

The hydrated salt **14,** mp 220−221°C, formed between **4** and (*S,S*)-tartaric acid, melted with decomposition and evolution of CO_2 like its diastereomer **13**. However, in the case of **14**, there was a clear loss of crystallinity around 100°C which reflects the loss of water molecules from the crystal lattice. X-ray analysis unambiguously showed that **14** includes two molecules of water of crystallization which are lost during drying under vacuum resulting in the disruption of the lattice.

The gaps opened in the crystal lattice of **14** as a result of an imperfect matching of partners are filled with the inclusion of two water molecules (Figure 11). One acceptor water molecule is hydrogen bonded to one hydroxyl; the other is bound as a donor to one carboxylate oxygen. Compared to the highly organized crystal structure of **13**, the structure of **14** shows that one hydroxyl−carboxylate bond has been disrupted and a corresponding coordination has been achieved with one water molecule each. Nevertheless, a layered structure of the core, the stacking of the cyclohexane residues, the "shelves on the wall" motif, and a hollow brick canal-like framework of the layer are surprisingly retained, although with a lower level of organization (Figure 11B). The thickness of the bilayered core is 4.50 Å; the width of the assembly is 13.50 Å including the cyclohexane residues, and the repeat distance between two shelves is 8.302 Å. What has been substantially altered in **14** compared to **13** is the connectivity pattern, because of hydrogen bonding to water. Apparently, the assembly of **14** cannot be sustained without the added water molecules and results in a loss of crystallinity by easy dehydration.

Discussion

We have demonstrated the unequivocal existence of unique supramolecular structures that result from the association of diamines and diols on the one hand and diamines and carboxylic acids on the other. Although H-bonding plays a primordial role in the process of self-assembly, the resulting three-dimensional structures are the consequence of a number of factors. The most compelling dilemma is to distinguish between two or more possible assembly scenarios. In the first, one could assume the existence of a preorganized arrangement of one of the components (e.g., the diamine) which would accommodate other partners (e.g., diols) in energetically most favorable terms, followed by a cascade of H-bonding interactions leading to the observed structures. A second possibility may involve an initial diamine−diol interaction through H-bonding to produce a "starter unit" (e.g., Figure 1A,B) followed by a spontaneous assembly of supramolecular entities by juxtaposition of other such units along preferred crystallographic coordinates, provided that symmetry, steric, and geometric requirements are satisfied. There may be other possibilities and combinations which are extremely difficult to delineate in view of the spontaneity of the process.

Before one concedes to the subtle forces that combine to produce the observed supramolecular assemblies, we must appreciate that H-bonding is being used in the most productive

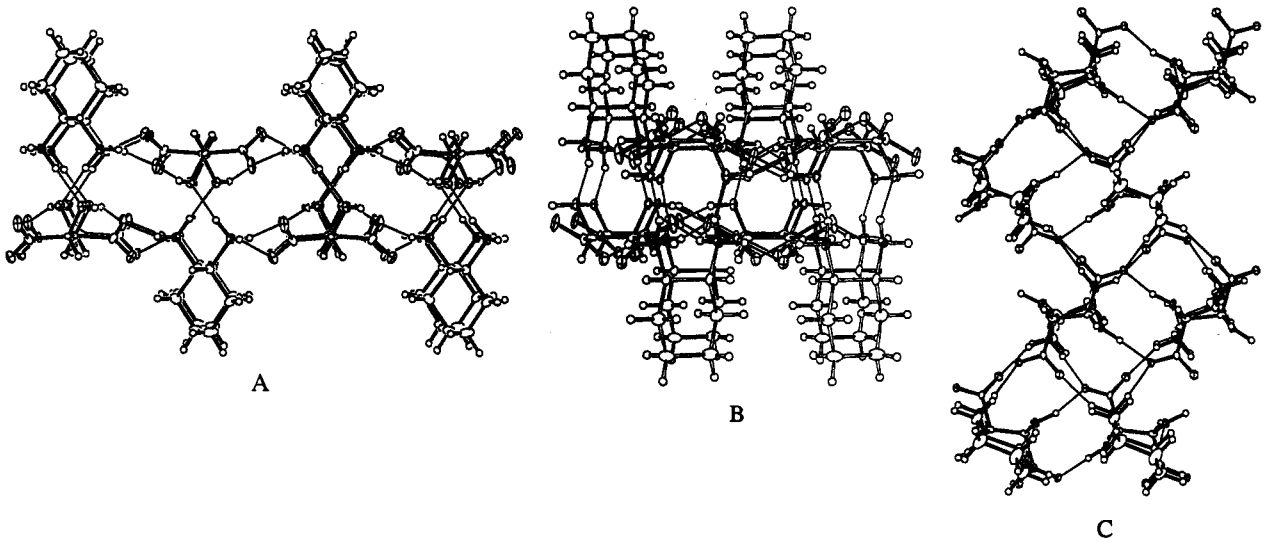

Figure 10. (A) Top view of **13** down the *a* axis, showing "tweezer"-shaped H-bonding between amino and hydroxy groups. (B) Side view of **13** down the *b* axis showing the bilayered core. (C) Side view down the *c* axis showing the H-bonded network.

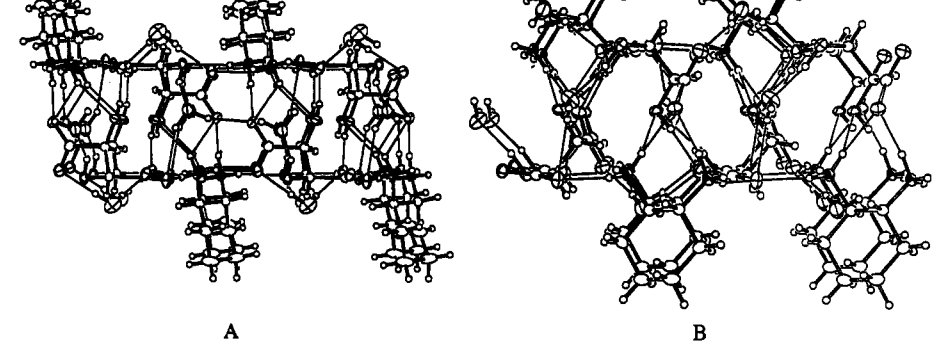

Figure 11. (A) Top view of **14** down the *b* axis showing two molecules of water bound to tartrate hydroxyl and carboxylate groups. (B) Side view of **14** down the *a* axis showing the H-bonded network.

manner to accommodate the interacting partners, regardless of accepted notions of donor–acceptor roles. For example, the role of OH as donor and NHR as acceptor has been amply documented,[19] and the donicity of groups has been rationalized on the basis of extensive comparisons.[20] The acceptor role of amines has been related to their basicities.[21]

The supramolecular structures described in this work have exhibited a variety of H-bonding interactions that range from OH donor–NHR acceptor (e.g., **3** strand, Figure 3A) to equally shared roles (e.g., **3** and **5** core, Figure 1C,F) to a reversal in the donicity mode, where NH acts as donor and OH as acceptor (e.g., **5** strand, Figure 3B) within allowed H-bond distances. It is noteworthy that **3** exhibits residues with left-handed helicity, while the reverse is seen in **5**, simply by using an enantiomeric diamine.

Other interesting features associated with the H-bonding pattern[22] in these supramolecular structures include the *direction* of the bond and the degree of *coordination*, which comprises full tetracoordination (e.g., **3** and **5** staircase cores, Figure 1C,F; **7**, Figure 4B) and tricoordination (e.g., **3** and **5** side rows, Figure 1G,H). We believe that the degree of coordination that maximizes the number of possible H-bonding interactions is the major driving force in the assembly of such supramolecular structures. While thermodynamic data exist for simple alcohols and amines (e.g., phenols and tertiary amines),[21] little is known of polyfunctional systems such as those reported here.[16] Thus, a combination of symmetry, steric, geometric, and electronic effects may be operative in the self-assembly of the diamine–diol motifs. The encoded stereochemical information of complementary functional groups is read by the recognition process that ultimately leads to superstructures exhibiting aesthetic beauty and unique three-dimensional architecture.

Neutral Networks. When the supramolecular architecture of neutral complexes is discussed, two different structural motifs must be distinguished and taken into account independently: first the motif of the hydrogen-bonded core and second the motif of the residues. Whenever perfect matching of the hydrogen-bonding capabilities of partners is allowed by their steric and geometric requirements, as with **7**, all the coordination vacancies of both heteroatoms are fulfilled and both the core and the residues assume helical motifs, with independent chirality senses (Figure 4B–D). This observation suggests that the helical arrangement is the most favorable arrangement for the hydrogen-bonded partners. Increasing the steric demand of residues, as in **3** and **5**, prevents the core from coiling into a helix. While

(19) See for example ref 8c, p. 272; ref 5b, p 133; and ref 3a, p 119.
(20) Abraham, M. H. *Chem. Soc. Rev.* **1993**, 73. Kamlet, M. J.; Abboud, J.-L. M.; Abraham, M. H.; Taft, R. W. *J. Org. Chem.* **1983**, *48*, 2877. Kamlet, M. J.; Abboud, J.-L. M.; Taft, R. W. *Prog. Phys. Org. Chem.* **1981**, *13*, 485.
(21) Arnett, E. M.; Mitchell, E. J.; Murty, T. S. S. R. *J. Am. Chem. Soc.* **1974**, *96*, 3875. See also ref 8c.
(22) For a discussion on H-bond patterns in organic compounds, see refs 3a and 4d.

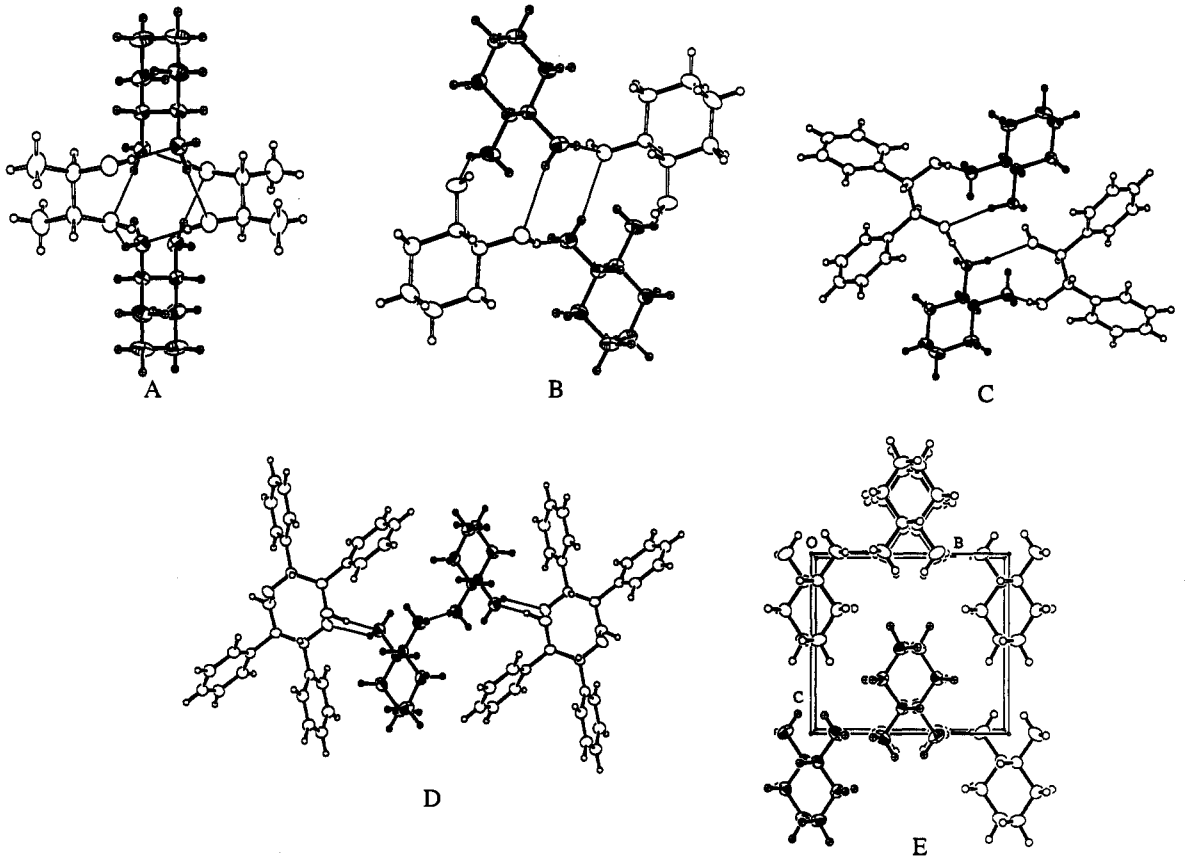

Figure 12. Comparison of the dispositions of the diaminocyclohexane molecules in the crystal lattice of **7** (A), **3** (B), **9** (C), and **11** (D) with that in **4** (E).

residues maintain their helical motif in these adducts, the core is not conducive to the formation of a helical ribbon-like motif, and prefers a pleated sheet staircase-like structure where heteroatoms are fully coordinated except in the side rows (Figure 1G,H). Further increase in the steric demand of residues progressively loosens hydrogen bonds, leading to an incompletely formed staircase-shaped core in **9** (Figure 5B,C), and opening up into a layered structure in its diastereomeric counterpart **11** (Figure 6B). Comparison of the described networks with the crystal lattice of the parent diamine **4** (Figure 12) suggests that the latter behaves as a *matrix* for self-assembly, regardless of the partner's structure, and provides a rationale for the observed architecture. The crystal lattice of the diamine dominates the inclusion of the diol partner, and becomes increasingly evident in the assembly, as the matching of partners becomes more imperfect, i.e., from **7** to **3** (and **5**) and to **9**, and eventually becomes conspicuous in **11** (Figure 12A–D). Lengthening of O–O distances, which follows the evolution of motifs in the core from helical ribbon (two short O–O distances, Figure 12A)to pleated sheet (one short and one long O–O distance, Figure 12B,C) to bidimensional layer (two long O–O distances, Figure 12D), parallels the increasing inability of the diol to fit into the diamine's lattice. Concurrently, the symmetry of the assembly decreases from **7** ($I2_12_12_1$) to **3** and **5** ($P2_12_12_1$) to **9** and **11** ($P2_1$). Eventually, the formation of only one of the two possible hydrogen bonds in the adduct **11** prevents the structure from assembling around a monodirectional core, with the incompletely formed helicate **9** constituting the transition architecture.

Control over dimensionality provided by tailored hydrogen-bonding networks is especially relevant in crystal engineering.[3,6e] From the above observations a corollary can be inferred, to be used in the design of supramolecular structures capable of self-assembling through molecular recognition between *trans*-1,2-diaminocyclohexanes and C_2 symmetrical diols. Whenever layered structures are desired, substituents on partners should be sterically hindered enough to prevent full coordination of heteroatoms and consequent generation of a monodirectional core. Conversely, helical cores are possible between diamine and diol residues with mutually compatible substituents of low steric demand. Helical arrangements of residues are still possible for substituents of moderate steric requirements. In general, formation of two hydrogen bonds in the adduct is a requirement for monodirectional networks, and the incorporation of a H-bonded core motif. A layered network requires the establishment of only one out of two possible hydrogen bonds. When either enantiomer of the diamine **1** or **4** is used as the *assembler* molecule, the helicity sense of the residues and the motif of the polar core of the assembly depend on the configuration of the diamine and the extent of H-bonding.

It may be anticipated that severe steric hindrance of substituents should hamper molecular recognition and assembly. This is indeed the case with a sterically congested *trans*-diol, i.e., 1,2:5,6-Di-*O*-cyclohexylidene-D-mannitol, which failed to form crystalline complexes with both enantiomers of the *assembler* **1**. As a control experiment, complex formation was attempted with (*R*)-1,1′-bi-2-naphthol, a hindered, high melting diol, which has been described to be resolved with **1** by the same procedure.[14] Although binaphthol is more acidic than the aliphatic diols employed in this work, thus more prone to form complexes, it failed to form crystals with **1** or **4** that were suitable for X-ray studies. A prerequisite for co-crystallization is the establishment of hydrogen-bonding interactions stronger than within the individual reagents themselves. The preference for cocrystallization exhibited by the diamines and diols described in this work can be related to the ability of the amine–hydroxyl pair to achieve an advantageous full tetrahedral coordination with each other, while this is constitutionally not

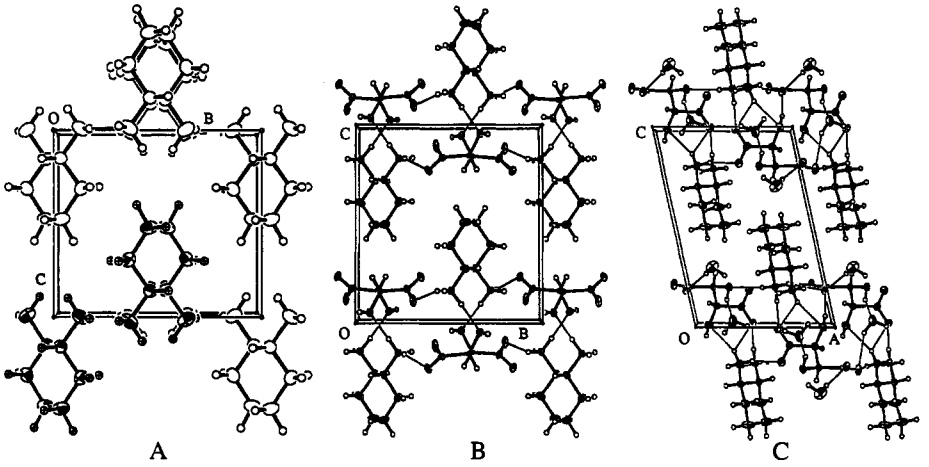

Figure 13. Comparison of the dispositions of the diaminocyclohexane molecules in the crystal lattice of **4** (A), **13** (B), and **14** (C). The similarity of the position of the diamine molecules in (B) to that in (A) is evident (molecules are shifted by 1/3 of the cell length along the *c* axis relative to one another). Distortion induced by imperfect matching and water molecules in the crystal lattice of **14** is shown in (C).

possible within the individual partners. The strength of the intramolecular hydrogen bond in *trans*-1,2-cyclohexanediol has been determined to be 1.93 kcal/mol.[16] Therefore, the free-energy gain involved in the described phenomena must be larger than this value to compete effectively, since smaller values would deter hydrogen bond-driven molecular recognition.

In conclusion, *trans*-1,2-diaminocyclohexane behaves as a unique *assembler* of supramolecular structures. The helicate motif seems to be a dominant feature of its architectural design. Inclusion of diol molecules into the matrix of its native crystal lattice seems to be governed by steric requirements, which finely modulate the achievement of molecular recognition between a well-matched pair of partners. In the present set of structures we were able to observe the whole range of molecular recognition between **1** (and **4**) and C_2 symmetrical diols, extending from the generation of tightly hydrogen-bonded and fully coordinated self-assemblies to the absence of complex formation between partners. It is not possible at this time to definitively distinguish between an inclusion hypothesis, where diols fit into the native crystal lattice of the diamine, and the spontaneous assembly of diamine−diol starter units. What is clear, however, is that the stereochemical information encoded in the complementary diamine−diol pair does lead to recognition and ultimately to spontaneous self-assembly in the favorably matched cases. Even with the relatively limited examples shown in this work, it is now possible to make logical predictions regarding supramolecular architecture from a knowledge of the structures of smaller components. Ironically, a major hurdle still remains in the suitability of the materials for X-ray crystallographic analysis.

Charged Networks. In contrast to the neutral helical networks in **3**, **5**, and **7**, the charged networks included in the present study showed a marked tendency to self-assemble into layered superstructures. Of particular interest, however, is **12** which consists of a layered superstructure consisting of helical elements that is unprecedented for this type of salt (Figure 2, bottom left).

Amidic-type and salt-type H-bonding can be envisaged in the assembly of **12**. Typical values of the CO bond lengths in standard hydrogen-bonded amides cluster around 1.23 ± 0.005 Å, while corresponding values for standard ammonium carboxylates are consistently around 1.25 Å. Two different CO bond lengths are observed in the carbamate **12**: 1.25 Å for the oxygen involved in the amidic-type hydrogen bonding and 1.28 Å for that engaged in the salt type. These values appear to be in line with those reported for simple ammonium carbamates of ammonia (1.28−1.29 Å)[23] and morpholine (1.25−1.27 Å),[24] suggesting not only strong hydrogen bonding but also a marked electrostatic character of the amidic-type bond. Correspondingly, a marked double bond character of the C−N bond is observed, which is reflected in the short C−N distance and in the perfect coplanarity of the rows involving amidic-type hydrogen bonds. Furthermore, bond angles around the carbonyl group are also informative, being within the standard values of a carboxylate anion, but different from the typical amidic values. In other words, charge is not localized on the oxygen bound to the ammonium cation, but tends to delocalize along the network (Scheme 2). Low temperature factors and good resolution of the crystal structures ensure the reliability of data.[15]

trans-1,2-Diaminocyclohexanes **1** and **4** have been resolved with tartaric acid,[18] but the inherent structural features of the resulting salts have not been investigated. The results of the present study provide some new insights into the structures of diastereomeric salts **13** and **14**. We have seen how different diols combine with the diamines **1** and **4** to provide three-dimensional superstructures as a result of molecular recognition and hydrogen bonding. As expected, carboxylate salts give stronger hydrogen bonding than diols because of a strong electrostatic attraction. An indication of this feature in the tartrate networks is provided by the relatively high calculated density of the crystals (**13**, D_{calcd} = 1.423; **14**, D_{calcd} = 1.391). In addition, the most conspicuous feature of the assembly is its resemblance to the lattice of diamine **4** (Figure 13A). The latter is superposable to the diamine part of the network of **13** (Figure 13B) by translation of alternate amine molecules by 1/3 of the cell length along the *c* axis, to leave a gap precisely occupied by a tartrate molecule. The minimal perturbation of the original diamine lattice, the highly compact packing of molecules, the perfect staggering of all bonds in the structure, and the orthogonality of carboxylate groups can be appreciated in the architecture of **13**. Such a compact assemblage may account for the high melting point of this highly organized solid superstructure. Interestingly the lattice of the hydrated salt **14** also exhibits the same relationship to that of the original diamine (Figure 13C). However, a good match between the two partners cannot be achieved, resulting in distortion of the cell, and inclusion of water molecules to fill the gaps. Hence, differences

(23) Adams, J.-M.; Small, R. W. H. *Acta Crystallogr.* **1973**, *B29*, 2317.
(24) (a) VonDreele, R. B.; Bradshaw, R. L.; Burke, W. J. *Acta Crystallogr.* **1983**, *C39*, 253. (b) Brown, C. J.; Gray, L. R. *Acta Crystallogr.* **1982**, *B38*, 2307. (c) Brown, C. J.; Gray, L. R. *Acta Crystallogr.* **1981**, *A37*, C202.

in solubility, stability, and melting points between **13** and **14** find a structural origin.

Thus, we believe that the actual driving force for the efficient resolution of the racemic diamine **1** with tartaric acid is the optimal molecular recognition that occurs between the matched pair of partners in the self-assembly of the supramolecular hydrogen-bonded structure.

It is of interest to compare the charged networks shown here with related examples in the area of engineered solids. A number of hydrogen-bonded networks have been reported for tartaric acid salts of organic amines,[25] which have been found to have nonlinear optical properties, and their activity for the second harmonic generation (SHG) has been related to the ability of assembling hydrogen-bonded charged arrays. Two important conclusions were inferred from the analysis of a significant set of structures: (a) The anions prefer specific aggregate structures, essentially independent of the charge and size of the cation. (b) They all show a marked tendency to form layered hydrogen-bonded structures.[25] The networks shown in the present study obtained using **4** as the *assembler* molecule demonstrate that the preference for a specific assemblage is governed by the parent diamine that acts as a matrix even in the presence of tartrate anions.

Molecular design of charged layered materials has attracted much attention in recent years and has been shown to be crucial for electronic properties such as non-linear optical activity and electronic conduction.[26] For example, guanidinium sulfonates have been reported as a novel class of solids for the synthesis of new electronic materials.[27] The specific structural features of the solid-state architectures based on the ammonium carboxylate functionality described in the present paper may open new perspectives in the field. In the same context, although the actual structure of the carbonated complexes resulting from **3** and **5** could not be established, their charged polymeric chemical constitution and their fibrous physical shape appear to be very promising for continued studies with related systems. The helical, layered superstructure of the carbamic acid salt **12** may be expected to induce interesting phenomena in the solid state. Since the requirements for nonlinear optical activity are fulfilled (SHG is only possible in noncentrosymmetric assemblies and in needle-shaped crystals),[25] we believe that the described charged networks can have potentially very interesting applications in the field of engineering of molecular solids.

Conclusion

The construction of supramolecular structures based on the ability of simple aliphatic diamines and diols to engage in molecular recognition solely by H-bonding opens up new vistas in the engineering of related solid-state structures. The most outstanding conclusion of the present work is that *trans*-1,2-diaminocyclohexane appears to be an exceptional *assembler* of both neutral and charged hydrogen-bonded networks, with C_2-symmetrical aliphatic diols, with carboxylic hydroxy acids, and even with itself by reacting with CO_2. In all cases, the crystal lattice of the diamine is evident in the architecture of the resulting supramolecular assembly. When helical motifs were obtained, the chirality sense of the helix consisting of outer residues or H-bonded cores could be anticipated from the absolute configuration of the *assembler* and the nature of the inner core (staircase- or ribbon-like). A new tool is thus available to control the way in which molecular units form aggregate superstructures through hydrogen bonding and to make reasonable predictions of the crystalline structures of such assemblies. This may eventually shed some light on the mechanisms that govern the molecular recognition codes in natural systems involving amines and complementary molecules.

Experimental Section

General Methods. All the starting materials used were commercial products whose physical constants were in agreement with reported values. Compounds **1** and **4** were obtained by a resolution process described in ref 18. Melting point determinations are uncorrected. NMR spectra were recorded at 300 and 400 MHz for ^1H and at 75 and 100 MHz for ^{13}C. For X-ray structure determination and additional data, see below and the supporting information.

General Procedure for Preparing Neutral Crystalline Adducts. Equimolar quantities of the diamines **1** or **4** and appropriate diols were suspended in dry benzene, and the suspension was heated to the boiling point on a hot plate. The homogeneous solution was allowed to cool to room temperature, whereupon crystalline adducts were formed in almost quantitative yield. These were filtered and recrystallized from benzene.

Adduct 3: colorless needles; mp 78−79 °C; $[\alpha]^{21}_D$ +38.2° (*c* 1, $CDCl_3$); ^1H NMR (0.22M, benzene-d_6) δ 0.88 (m, 1H, CH_2CH$_2$CHN), 1.08 (m, 1H, CH_2CH$_2$CHN), 1.15 (m, 1H, CH_2CH$_2$CHO), 1.42 (m, 1H, CH_2CH$_2$CHO), 1.50 (m, 1H,CH_2CHN), 1.52 (m, 1H, CH_2CHO), 1.60 (m, 1H, CH_2CHN), 1.98 (m, 1H, C*H*N), 2.05 (m, 1H, CH_2CHO), 2.55 (brs, 3H, OH + NH_2), 3.50 (m, 1H, C*H*O); ^{13}C NMR (0.22 M, benzene-d_6) δ 24.97 (*C*H$_2$CH$_2$CHO), 25.76 (*C*H$_2$CH$_2$CHN), 33.79 (*C*H$_2$CHO), 35.84 (*C*H$_2$CHN), 57.58 (*C*HN), 75.79 (*C*HO).

Adduct 5: colorless needles; mp 63−65 °C; $[\alpha]^{21}_D$ −1° (*c* 1, $CDCl_3$); ^1H NMR (0.21 M, benzene-d_6) 0.88 (m, 1H, CH_2CH$_2$CHN), 1.08 (m, 1H, CH_2CH$_2$CHN), 1.15 (m, 1H, CH_2CH$_2$CHO), 1.42 (m, 1H, CH_2CH$_2$CHO), 1.50 (m, 1H, CH_2CHN), 1.52 (m, 1H, CH_2CHO), 1.60 (m, 1H, CH_2CHN), 1.98 (m, 1H, C*H*N), 2.05 (m, 1H, CH_2CHO), 2.60 (brs, 3H, OH + NH_2), 3.50 (m, 1H, C*H*O); ^{13}C NMR (0.21 M, benzene-d_6) δ 24.98 (*C*H$_2$CH$_2$CHO), 25.70 (*C*H$_2$CH$_2$CHN), 33.68 (*C*H$_2$CHO), 35.76 (*C*H$_2$CHN), 57.43 (*C*HN), 75.85 (*C*HO).

Adduct 7: colorless rods; mp 65−67 °C; $[\alpha]^{25}_D$ −32.4° (*c* 1.2, $CDCl_3$); ^1H NMR (0.1 M, $CDCl_3$) δ 1.10 (m, 1H, CH_2CH$_2$CHN), 1.13 (d, J = 5.6, 3H, CH_3), 1.24 (m, 1H, CH_2CH$_2$CHN), 1.66 (m, 1H, CH_2CHN), 1.81 (m, 1H, CH_2CHN), 2.23 (m, 1H, C*H*N), 3.45 (m, 1H, C*H*O); ^{13}C NMR (0.1 M, $CDCl_3$) δ 19.31 (CH_3), 25.33 (*C*H$_2$CH$_2$CHN), 35.56 (*C*H$_2$CHN), 57.50 (*C*HN), 72.18 (CHO).

Adduct 9: colorless plates; mp 75−76 °C; $[\alpha]^{25}_D$ +44.6° (*c* 1.8, $CDCl_3$); ^1H NMR (0.1 M, $CDCl_3$) δ 1.00 (m, 1H, CH_2CH$_2$CHN), 1.18 (m, 1H, CH_2CH$_2$CHN), 1.62 (m, 1H, CH_2CHN), 1.72 (m, 1H, CH_2CHN), 2.10 (m, 1H, C*H*N), 4.61 (s, 1H, C*H*O), 7.06−7.24 (m, 5H, Ph); ^{13}C NMR (0.1 M, $CDCl_3$) δ 25.26 (*C*H$_2$CH$_2$CHN), 35.33 (*C*H$_2$CHN), 57.24 (*C*HN), 78.77 (CHO), 126.98, 127,84 (C-2, C-3, Ar), 127.45 (C-4, Ar), 140.70 (C-1, Ar).

Adduct 11: colorless plates; mp 99−100 °C; $[\alpha]^{25}_D$ −71.5° (*c* 2.1, $CDCl_3$); ^1H NMR (0.1 M, $CDCl_3$) δ 1.02 (m, 1H, CH_2CH$_2$CHN), 1.19 (m, 1H, CH_2CH$_2$CHN), 1.63 (m, 1H, CH_2CHN), 1.74 (m, 1H, CH_2CHN), 2.14 (m, 1H, C*H*N), 4.62 (s, 1H, C*H*O), 7.08−7.24 (m, 5H, Ph); ^{13}C NMR (0.1 M, $CDCl_3$) δ 25.27 (*C*H$_2$CH$_2$CHN), 35.32 (*C*H$_2$CHN), 57.27 (*C*HN), 78.86 (CHO), 126.98, 127.86 (C-2, C-3, Ar), 127.48 (C-4, Ar), 140.60 (C-1, Ar).

Adduct 12: A quantity of **4** (115 mg) was exposed to dry ice in a desiccator for 24 h, after which it was transformed into a nonhygroscopic off-white powder (152 mg) that melted with evolution of CO_2. The weight increase and elemental analysis were in accord with the absorption of an equivalent quantity of CO_2. Single crystals were obtained by addition of ethanol to an aqueous solution of the solid: colorless needles; mp 142−155 °C dec (with CO_2 evolution); $[\alpha]^{25}_D$ −33.5° (*c* 0.4, D_2O); ^1H NMR (0.06 M, D_2O) δ 1.18−1.38 (m, 4H, CH_2CH$_2$CHN), 1.68−1.76 (m, 2H, CH_2CHN), 1.85−2.02 (m, 2H, CH_2CHN), 2.58 (m, 1H, C*H*N), 3.15 (m, 1H, C*H*N); ^{13}C NMR (0.06 M,

(25) Aakeröy, C. B.; Hitchcock, P. B.; Seddon, K. R. *J. Chem. Soc., Chem. Commun.* **1992**, 553. Aakeröy, C. B.; Hitchcock, P. B.; Moyle, B. D.; Seddon, K. R. *J. Chem. Soc., Chem. Commun.* **1989**, 1856.

(26) *Materials for Nonlinear Optics*; Marder, S. R., Sohn, J. E., Stucky, G. D., Eds.; ACS Symposium Series 455; American Chemical Society: Washington, DC, 1991.

(27) Russell, V. A.; Etter, M. C.; Ward, M. D. *J. Am. Chem. Soc.* **1994**, *116*, 1941.

D_2O) δ 24.83 (CH_2CH_2CHN), 25.31 (CH_2CH_2CHN), 32.87 (CH_2CHN), 33.25 (CH_2CHN), 54.90 (CHN), 56.83 (CHN), 165.13 (COO).

Reaction of 3 and 5 with CO_2. Reaction of adducts **3** and **5** with CO_2 was first observed as a gradual carbonation of crystals exposed to air. The crystals of **3**, originally used for X-rays, were no longer crystalline after four months. They preserved the outer shape of crystals but did not diffract X-rays, and melted at 170−180 °C, with evolution of CO_2 that began at 118 °C. Elemental analysis (found: C, 57.26; H, 9.86; N, 10.03) of this sample was in good agreement with that of a compound formed by the addition of 1 equiv of CO_2 to the complex **3**. The phenomenon could be reproduced by forced carbonation. A sample was melted and allowed to solidify at room temperature, and its melting point was redetermined to give 74−75 °C with no evolution of gas, and no melting point depression with a sample of **3**.

A solid sample of **3** was exposed to CO_2 for a few days, and the adduct was analyzed by ^1H and ^{13}C NMR spectroscopy which showed that 33% of the adduct had been converted into the carbamate salt **12**, while the signals of the diol **2** appeared unchanged. The partially carbonated complex melted over a wide range of temperatures, 62−65 °C (partial), then 118−122 °C, and 165−173 °C (melting with evolution of CO_2). Crystallization of a sample from ethanol/water gave crystals of **12**, mp 140−145 °C dec (with CO_2 evolution).

Adduct 13: colorless plates (from water); mp 252−255 °C dec (with CO_2 evolution); $[\alpha]^{25}_D$ +11.6° (*c* 1.1, H_2O) [lit.[18] $[\alpha]^{25}_D$ +11.6° (*c* 1.0, H_2O)]; ^1H NMR (saturated solution, <0.1 M, D_2O) δ 1.32 (m, 1H, CH_2CH_2CHN), 1.50 (m, 1H, CH_2CH_2CHN), 1.78 (m, 1H, CH_2CHN), 2.12 (m, 1H, CH_2CHN), 3.34 (m, 1H, CHN), 4.32 (s, 1H, CHO); ^{13}C NMR (saturated solution, <0.1 M, D_2O) δ 25.55 (CH_2CH_2CHN), 32.11 (CH_2CHN), 54.90 (CHN), 76.62 (CHO), 181.29 (COO).

Adduct 14: colorless plates (from water); mp 220−221 °C dec (with CO_2 evolution); $[\alpha]^{25}_D$ −35.8° (*c* 1.3, H_2O);[18] ^1H NMR (0.1 M, D_2O) δ 1.32 (m, 1H, CH_2CH_2CHN), 1.48 (m, 1H, CH_2CH_2CHN), 1.80 (m, 1H, CH_2CHN), 2.12 (m, 1H, CH_2CHN), 3.32 (m, 1H, CHN), 4.32 (s, 1H, CHO); ^{13}C NMR (0.1 M, D_2O) δ 25.61 (CH_2CH_2CHN), 32.26 (CH_2CHN), 55.03 (CHN), 76.63 (CHO), 181.32 (COO).

Crystallographic Data. Single crystals of **3**, **5**, **7**, **9**, and **11** were obtained by crystallization from benzene as described above. Single crystals of **13** were obtained by crystallization from hot water and those of **14** by slow evaporation of a water solution at room temperature. Oversized crystals of suitable quality were cut to adequate dimensions by the scalpel technique. The two tartrate salts **13** and **14** showed twinning problems occurring by stacking of two plates of related orientation, and were resolved by cutting along the edge of the plates, parallel to the large faces. Crystals of **12** were obtained from ethanol/water as described above. Table 1 contains pertinent crystallographic data for adducts **3**, **5**, **7**, **9**, and **11**−**14**. See also the supporting information. Tables of final atomic coordinates, anisotropic temperature factors, distances, angles, torsion angles, and hydrogen bond distances and angles for compounds **7**, **9**, and **11**−**14** have been deposited at the Cambridge Crystallographic Data Centre.

Collection and Reduction of the Data. X-ray intensity data were collected at 215 K on an Enraf-Nonius CAD-4 diffractometer employing graphite-monochromated Cu Kα radiation (λ = 1.540 56 Å) with use of the ω−2θ scan technique. For each compound a minimum of three standard reflections measured every 1/2 h of X-ray exposure showed less than ±5% intensity decay over the course of data collection. A linear decay correction was applied. The intensity data were corrected for Lorentz and polarization effects, but not for absorption.

Solution and Refinement of the Structure. All calculations were performed using the NRCVAX structure package, compound **12** and **13** excepted, which were processed using the SHELX-76 program system. All the reported architectures exhibited remarkably low disorder, as can be inferred from temperature factors of the refined crystal structures (see the supporting information). The full-matrix least-squares refinement was based on *F*, and the function minimized was $w(|F_o| - |F_c|)^2$. The weights applied were $w^{-1} = \sigma^2(F)^2(F_o) + 0.0001(F_o)^2$ where $|F_o|$ and $|F_c|$ are the observed and calculated structure factor amplitudes. The neutral atom scattering factors and complex anomalous dispersion corrections are those stored in the NRCVAX (or SHELX76) package. Agreement factors are defined as $R_f = (||F_o| - |F_c||)/(|F_o|)$, $R_w = [w(|F_o| - |F_c|)^2/(w|F_o|^2)]^{1/2}$ and GoF = $[|F_o| - |F_c|)^2/$(no. of reflns − no. of params)]$^{1/2}$. The structures were solved by direct methods (SHELXS-86). The enantiomorph was fixed from known absolute configuration (*R*,*R*) of the starting material **4** and then confirmed by a Bijvoet analysis of the Friedel pair reflections. All non-hydrogen atoms were located from the first E-map. Subsequent Fourier maps led to the location of all hydrogen atoms related to the hydrogen-bonding networks. All others hydrogen atoms were initially calculated at idealized positions (d_{C-H} = 0.95 Å) and were refined in the last cycles. Anisotropic refinement was applied to all non-hydrogen atoms. The dispersion contribution was included for oxygen and nitrogen atoms. Final difference Fourier maps were featureless.

Crystal and refinement data, selected distances, and angles related to the hydrogen-bonding networks are included in the supporting information.

Acknowledgment. We acknowledge generous financial assistance from NSERCC and Le Ministère de l'Éducation and greatly appreciate a sabbatical leave for S.R. (CNR, Florence, Italy). We thank Benoit Larouche for his invaluable assistance in the preparation of the artwork presented in this paper. We also thank Dr. A. Gomtsyan for his valuable contributions at the inception of the project, and for the sublimation experiments.

Supporting Information Available: Tables giving the crystallographic data, refined coordinates, temperature factors, hydrogen atom coordinates, anisotropic thermal parameters, bond distances and angles, and torsion angles for **7**, **9**, and **11**−**14** and least-squares plane calculations for **9** and **11** and figures showing the numbering scheme, hydrogen bonding network, and stereoview of the cell for **7**, **9**, and **11**−**14** (98 pages). This material is contained in many libraries on microfiche, immediately follows this article in the microfilm version of the journal, can be ordered from the ACS, and can be downloaded from the Internet; see any current masthead page for ordering information and Internet access instructions.

JA950266J